



Publication Year	2018
Acceptance in OA @INAF	2021-01-26T13:32:18Z
Title	The Hubble Space Telescope UV Legacy Survey of Galactic globular clusters - XIII. ACS/WFC parallel-field catalogues
Authors	Simioni, Matteo; BEDIN, Luigi; Aparicio, A.; Piotto, G.; Milone, A. P.; et al.
DOI	10.1093/mnras/sty177
Handle	http://hdl.handle.net/20.500.12386/30006
Journal	MONTHLY NOTICES OF THE ROYAL ASTRONOMICAL SOCIETY
Number	476

The *Hubble Space Telescope* UV Legacy Survey of Galactic Globular Clusters. XIII. ACS/WFC Parallel-Field Catalogues[★]

M. Simioni^{1,2,3,4,†}, L. R. Bedin⁴, A. Aparicio^{2,1}, G. Piotto^{3,4}, A. P. Milone^{3,5},
D. Nardiello^{3,4}, J. Anderson⁶, A. Bellini⁶, T. M. Brown⁶, S. Cassisi^{7,1}, A. Cunial³,
V. Granata^{3,4}, S. Ortolani^{3,4}, R. P. van der Marel^{6,8}, E. Vesperini⁹

¹*Instituto de Astrofísica de Canarias, E-38200 La Laguna, Tenerife, Canary Islands, Spain*

²*Department of Astrophysics, University of La Laguna, E-38200 La Laguna, Tenerife, Canary Islands, Spain*

³*Dipartimento di Fisica e Astronomia “Galileo Galilei”, Università degli Studi di Padova, Vicolo dell’Osservatorio 3, Padova IT-35122*

⁴*INAF - Osservatorio Astronomico di Padova, Vicolo dell’Osservatorio 5, I-35122 Padova, Italy*

⁵*Research School of Astronomy and Astrophysics, Australian National University, Cotter Road, Weston, ACT 2611, Australia*

⁶*Space Telescope Science Institute, 3700 San Martin Dr., Baltimore, MD 21218, USA*

⁷*INAF - Osservatorio Astronomico di Teramo, Via M. Maggini, I-64100 Teramo, Italy*

⁸*Center for Astrophysical Sciences, Department of Physics & Astronomy, Johns Hopkins University, Baltimore, MD 21218, USA*

⁹*Department of Astronomy, Indiana University, Bloomington, IN47401, USA*

Accepted 2018 January 17. Received 2018 January 17; in original form 2017 October 10

ABSTRACT

As part of the *Hubble Space Telescope* UV Legacy Survey of Galactic Globular Clusters, 110 parallel fields were observed with the Wide Field Channel of the Advanced Camera for Surveys, in the outskirts of 48 globular clusters, plus the open cluster NGC 6791. Totalling about 0.3 square degrees of observed sky, this is the largest homogeneous *Hubble Space Telescope* photometric survey of Galactic globular clusters outskirts to date. In particular, two distinct pointings have been obtained for each target on average, all centred at about 6.5 arcmin from the cluster centre, thus covering a mean area of about 23 arcmin² for each globular cluster. For each field, at least one exposure in both F475W and F814W filters was collected. In this work, we publicly release the astrometric and photometric catalogues and the astrometrised atlases for each of these fields.

Key words: globular clusters: general – Hertzsprung-Russel and colour-magnitude diagrams; catalogues and atlases.

1 INTRODUCTION

For almost three decades, the Milky Way Globular Clusters (GCs) have been the target of large CCD photometric surveys aimed at sampling their stellar populations in a homogeneous way (Rosenberg et al. 2000a, Rosenberg et al. 2000b, Piotto et al. 2002, Sarajedini et al. 2007) using both space- and ground-based instruments. The growing sample of data, and the advent of increasingly sophisticated data-analysis techniques, have clearly demonstrated that

GCs host distinct stellar populations with different chemical abundances. High-precision photometric measurements have revealed that the colour-magnitude diagrams (CMDs) show distinct sequences in various evolutionary stages (see e.g. Anderson 1997, Lee et al. 1999, Pancino et al. 2000, Bedin et al. 2004, Piotto et al. 2007, Milone et al. 2008, Bellini et al. 2010). These findings are also supported by spectroscopical evidence that the stellar populations of these systems are not as simple as thought (see e.g. Marino et al. 2008, Yong & Grundahl 2008, Kraft 1994, Carretta et al. 2009a, Carretta et al. 2009b, Gratton et al. 2004, Gratton et al. 2012).

The *Hubble Space Telescope* UV Legacy Survey of Galactic Globular Clusters (GO-13297; PI:Piotto) has been specifically designed to further investigate this phenomenon

[★] Based on observations with the NASA/ESA *Hubble Space Telescope*, obtained at the Space Telescope Science Institute, which is operated by AURA, Inc., under NASA contract NAS 5–26555.

[†] email: msimioni@iac.es

and it now appears likely that all Galactic GCs host multiple stellar populations (Piotto et al. 2015 – hereafter *Paper I*, Milone et al. 2017 – hereafter *Paper IX*). In the context of this survey, parallel Advanced Camera for Surveys (ACS) observations have been obtained. While the main observations were taken using a combination of UV and optical filters of the Wide Field Camera 3 (WFC3), the lack of filters bluer than F435W dictated the use of the F475W and F814W filters of the Wide Field Channel of the ACS (ACS/WFC) in the parallel observations. The large colour baseline provided by this filter combination guarantees sensitivity to helium abundance differences, while being largely insensitive to star-to-star variations in light-element abundances (Sbordone et al. 2011, Cassisi et al. 2017).

One of the main objectives for which these observations were planned is to investigate how different stellar populations formed in GCs. Strong observational constraints come from the analysis of the radial distribution of each stellar population (D’Ercole et al. 2008; Bellini et al. 2009, Vesperini et al. 2013). As an example, Simioni et al. (2016) complemented WFC3 data of the central regions of NGC 2808 with ACS parallel observations and found evidence of different radial trends associated with distinct stellar populations hosted by the cluster. Thus, clusters with large helium variations among their stellar populations are the preferred target of investigation with the current data-sample. Other interesting targets, albeit extensively studied, are those defined as Type-II clusters in *Paper IX*, which displays multiple sub-giant branches in optical CMDs.

We stress the fact that this is the first homogeneous *HST* photometric survey of the outskirts of Galactic GCs. The observations presented here represent a first epoch for future studies aimed at systematical measurements of absolute, relative and internal proper motions of stars in these regions. Archival *HST* observations matching a sub-sample of the observed fields exist, and proper motions will be published separately. In the imaged stellar fields, the stellar density is not as high as in the central regions. As a consequence, crowding is not a serious issue for these data. That makes them particularly suitable to be used as input catalogue for future spectroscopic surveys.

The present catalogues can be used to perform several interesting analyses. For example, dynamical interactions between stars in GCs is at the origin of the mass segregation phenomenon. A precise estimate of its effects is fundamental for the derivation of a global mass function for a GC (Vesperini & Heggie 1997, Paust et al. 2010, Sollima & Baumgardt 2017). The measurement of the fraction of binaries is also fundamental for this kind of analysis and could provide useful constraints for dynamical models (Milone et al. 2012). We note, also, that in some cases white dwarf cooling sequences are visible in the obtained CMDs. Finally, it is interesting to note that due to the presence of many extragalactic objects in the observed field, other studies could benefit from these observations.

In this work, we present the first photometric catalogues from the ACS/WFC parallel observations of the GO-13297 program. All data have been reduced in a homogeneous manner, making these catalogues particularly suitable for inter-comparison. The article is organised as follows: in Section 2 the data are presented along with some information about the observing strategy, together with a detailed description

of the data reduction. The extracted CMDs are presented in Section 3. Details on the selection of well measured stars are given in Section 4. In Section 5 the catalogues and the released electronic material are described in detail. Finally, in Section 6, after a summary, we briefly discuss some of the main scientific questions we will address with these catalogues in subsequent papers.

2 OBSERVATIONS AND DATA REDUCTION

Tables 1 and 2 report the log of ACS/WFC observations used to construct the catalogues. For each target, we indicate the total number of orbits assigned to each observed field separated by the different position angles (PAs) of the V3 axis of the *HST* focal plane. Typically, one F475W and one F814W image were taken each orbit, with a dither between the two dictated by primary WFC3 observing strategy. For each field, right ascension and declination of the centre of ACS/WFC are provided along with exposure time in each filter.

The physical position of ACS/WFC detectors in the focal plane of *HST* is such that its projected field of view (FoV) in the sky is located at a distance of about 6.5 arcminutes from the centre of the WFC3 FoV. Depending on the number of orbits allocated to each GC, from 2 to a maximum of 5 non-overlapping fields were observed. This is because, in order to secure a good handling of charge-transfer-efficiency (CTE) systematic errors, primary WFC3 observations were taken by applying a different telescope rotation at each orbit (*Paper I*, Section 4). For the majority of clusters, which were allocated 2 orbits, a rotation of about 90° was performed between the first and second orbit; for clusters observed for more than 2 orbits, a minimum difference of $\sim 45^\circ$ between the V3 PA of each orbit was required. Five distinct pointings were obtained for 3 clusters, namely NGC 1261, NGC 5053 and NGC 6101. Three distinct fields were obtained for 4 clusters: NGC 6652, NGC 6717, NGC 6723 and NGC 7089. For the other clusters, only 2 pointings were planned. M80 is an exception and was not observed as part of the Program GO-13297. For it, we make use of archival *HST* data from GO-12311. When possible, ACS parallel observations targeted pre-existing *HST* observations.

Figures 1 and A1 – A8 display all *HST* observations that sample the sky area in the vicinity of those covered in this survey. Three cameras onboard *HST* were considered in order to enhance the probability of an overlap between observations: Wide Field and Planetary Camera 2 (WFPC2), ACS and WFC3 (both UVIS and IR channels). Taking 2 images per orbit, one in F475W and one in F814W filters, the typical exposure times for both filters are of the order of 700s.

All exposures have been corrected for CTE effects using the method described in Anderson & Bedin (2010). Photometric measurements of stellar objects in each field have been performed using a suite of FORTRAN programs based on `img2xym` (Anderson & King 2006) and `kitchen_sync` presented in Anderson et al. (2008). The spatial variation of the PSF has been taken into account adopting a grid of 9×10 model PSFs distributed along each image. However focus changes/breathing of the telescope, imperfect guiding, residual noise related to CTE can produce image-to-image

Table 1. Observation log. For each GC in the survey, and the open cluster NGC 6791,

we show right ascension and declination of each distinct parallel field, referred to the centre of ACS/WFC. We also report the number of orbits, Telescope orientation (V3 PA) for each orbit and exposure time in each filter.

#	CLUSTER	ORBITS	FIELD [PA (deg)]	RA (J2000) (^h ^m ^s)	DEC (J2000) ([°] ['] ^{''})	EPOCH	EXP. TIME F475W (s)	EXP. TIME F814W (s)
01	NGC1261	5	F1 [92]	03:12:49.68	-55:17:25.2	31/08/13	770	694
			F2 [138]	03:12:16.96	-55:19:29.6	11/09/13	745	669
			F3 [182]	03:11:44.35	-55:17:39.3	08/11/13	766	690
			F4 [225]	03:11:30.53	-55:13:17.9	07/12/13	745	669
			F5 [48]	03:13:01.92	-55:12:51.4	29/06/14	829	753
02	NGC1851	7	F1 [195]	05:13:37.57	-40:06:44.0	27/12/10	2x40;2x1277;1237	6x488;1x40
			F2 [164]	05:13:51.57	-40:08:55.8	11/11/10	2x40;2x1277;2x1237	8x488;2x40
03	NGC2298	4	F1 [185]	06:48:36.04	-36:05:08.7	18/12/13	2x785	2x683
			F2 [273]	06:48:35.14	-35:55:40.7	07/03/14	885	816
04	NGC3201	2	F1 [25]	10:18:12.19	-46:21:47.1	13/09/13	685	612
			F2 [115]	10:17:54.00	-46:30:51.0	01/01/14	689	616
05	NGC4590	2	F1 [112]	12:39:42.64	-26:50:34.9	21/12/13	627	554
			F2 [202]	12:39:01.10	-26:47:48.5	30/03/14	627	554
06	NGC4833	4	F1 [113]	13:00:10.12	-70:58:29.4	17/01/14	2x840	2x771
			F2 [202]	12:58:20.68	-70:55:42.6	09/04/14	2x806	2x730
07	NGC5024	6	F1 [31]	13:13:21.59	+18:12:01.1	24/03/14	4x725;2x723	3x370
			F2 [120]	13:13:03.82	18:03:52.0	08/12/13	4x775;2x774	3x375
08	NGC5053	5	F1 [352]	13:16:42.03	+17:47:28.7	01/04/14	740	664
			F2 [37]	13:16:53.97	+17:43:15.0	16/03/14	740	664
			F3 [80]	13:16:50.28	+17:38:33.1	23/01/14	790	714
			F4 [125]	13:16:33.21	+17:35:39.5	05/12/13	790	714
			F5 [308]	13:16:21.88	+17:48:25.0	16/05/14	765	689
09	NGC5286	2	F1 [73]	13:47:07.09	-51:25:00.2	14/12/13	728	655
			F2 [162]	13:46:11.09	-51:28:46.7	15/03/14	603	559
10	NGC5466	4	F1 [112]	14:05:41.08	+28:26:12.1	05/01/14	834;835	763;765
			F2 [21]	14:05:54.29	+28:35:18.1	29/03/14	2x776	2x700
11	NGC5897	4	F1 [112]	15:17:37.48	-21:06:27.5	12/02/14	830;833	2x761
			F2 [202]	15:16:58.75	-21:03:44.3	13/05/14	779;781	710;709
12	NGC5904	2	F1 [323]	15:18:34.23	02:11:38.3	17/05/14	620	559
			F2 [52]	15:19:00.34	02:04:36.4	08/04/14	621	559
13	NGC5927	3	F1 [100]	15:28:28.73	-50:45:30.4	01/02/14	603	559
			F2 [189]	15:27:28.26	-50:44:48.7	19/05/14	603	559
14	NGC5986	3	F1 [92]	15:46:28.87	-37:51:38.6	27/01/14	676	603
			F2 [180]	15:45:40.83	-37:52:21.9	17/05/14	603	559
						10/05/15	603	559
15	NGC6093	5	F1 [255]	16:16:35.04	-22:55:45.9	09/06/12	5x760;5x845	5x539
16	NGC6101	5	F1 [147]	16:25:36.08	-72:18:35.2	04/04/14	762	686
			F2 [190]	16:24:40.57	-72:16:07.7	25/05/14	762	686
			F3 [235]	16:24:23.48	-72:11:18.6	29/06/14	800	724
			F4 [282]	16:24:58.26	-72:06:50.7	14/08/13	851	775
			F5 [101]	16:26:39.71	-72:17:19.9	28/02/14	800	724
17	NGC6121	2	F1 [272]	16:23:12.57	-26:27:02.1	06/07/14	739	666
			F2 [98]	16:23:55.64	-26:36:33.4	17/02/15	666	593
18	NGC6144	2	F1 [83]	16:27:39.42	-26:05:00.9	28/02/14	679	606
			F2 [174]	16:26:57.33	-26:07:05.2	27/05/14	679	606
19	NGC6171	4	F1 [342]	16:32:41.94	-12:56:56.1	31/05/14	830;833	2x761
			F2 [72]	16:32:42.20	-12:57:07.5	25/03/14	800;802	731;730
20	NGC6218	2	F1 [276]	16:46:55.21	-01:52:03.7	16/08/13	721	648
			F2 [6]	16:47:33.42	-01:52:07.7	27/05/14	645	572
21	NGC6254	2	F1 [276]	16:56:50.04	-04:01:10.1	16/08/13	721	648
			F2 [7]	16:57:28.66	-04:01:19.2	27/05/14	644	571
22	NGC6304	2	F1 [184]	17:14:10.53	-29:32:35.1	07/06/14	624	559
			F2 [274]	17:14:09.53	-29:23:04.8	26/08/13	731	658
23	NGC6341	2	F1 [230]	17:16:30.21	+43:08:03.0	22/10/13	638	565
			F2 [319]	17:17:06.19	+43:14:56.0	03/08/14	750	677
24	NGC6352	2	F1 [161]	17:25:15.00	-48:31:41.7	27/05/14	637	564
			F2 [251]	17:24:51.02	-48:22:52.5	13/08/13	731	658

Continued on Tab. 2

Table 2. Table 1 (continued)

#	CLUSTER	ORBITS	FIELD [PA (deg)]	RA (J2000) (<i>h m s</i>)	DEC (J2000) (<i>° ′ ″</i>)	EPOCH	EXP. TIME F475W (s)	EXP. TIME F814W (s)
25	NGC6362	2	F1 [125]	17:32:14.07	-67:09:25.3	30/03/14	651	578
			F2 [215]	17:30:47.67	-67:04:37.3	01/07/14	760	687
26	NGC6366	2	F1 [293]	17:27:31.94	-04:58:44.4	26/08/13	726	653
			F2 [351]	17:27:58.09	-04:58:57.1	07/06/15	644	571
27	NGC6388	4	F1 [238]	17:35:40.80	-44:43:02.9	05/07/14	865;906	796;834
			F2 [141]	17:36:17.23	-44:50:53.5	12/05/14	793;795	724;723
28	NGC6397	2	F1 [90]	17:41:17.47	-53:44:46.1	27/03/14	683	610
			F2 [180]	17:40:12.50	-53:45:38.3	11/06/14	640	567
29	NGC6441	4	F1 [102]	17:50:34.23	-37:08:21.5	26/03/14	833;835	764;763
			F2 [192]	17:49:46.24	-37:07:12.6	15/06/14	2x794	725;722
30	NGC6496	2	F1 [157]	17:58:53.12	-44:22:28.2	30/05/14	638	656
			F2 [247]	17:58:27.50	-44:13:57.0	12/08/13	731	658
31	NGC6535	2	F1 [319]	18:03:49.95	+00:11:04.6	19/07/14	724	651
			F2 [50]	18:04:17.63	+00:17:50.2	26/05/14	644	571
32	NGC6541	2	F1 [80]	18:08:35.16	-43:46:11.5	14/02/14	689	616
			F2 [170]	18:07:44.04	-43:48:48.8	11/06/14	639	566
33	NGC6584	2	F1 [155]	18:18:26.74	-52:19:31.3	30/05/14	640	567
			F2 [245]	18:17:54.89	-52:11:09.9	18/08/13	726	653
34	NGC6624	2	F1 [264]	18:23:14.50	-30:17:51.1	03/09/13	731	658
			F2 [174]	18:23:23.29	-30:27:20.2	27/06/14	638	565
35	NGC6637	4	F1 [84]	18:31:49.55	-32:24:40.9	18/02/14	827;840	758;768
			F2 [174]	18:31:05.49	-32:26:31.5	30/06/14	792;794	723;722
36	NGC6652	3	F1 [281]	18:35:25.09	-32:54:08.8	30/08/13	707	633
			F2 [238]	18:35:14.87	-32:58:25.1	14/08/13	733	658
			F3 [192]	18:35:20.06	-33:03:36.1	01/07/14	621	548
37	NGC6656	4	F1 [266]	18:36:00.25	-23:50:16.5	23/09/10	656;644	2x389
			F2 [85]	18:36:47.76	-23:58:08.0	17/03/11	2x656	2x389
38	NGC6681	2	F1 [271]	18:42:48.78	-32:13:03.7	05/09/13	730	658
			F2 [183]	18:42:51.19	-32:22:33.1	29/06/14	637	564
39	NGC6715	6	F1 [153]	18:54:56.04	-30:35:08.9	29/06/14	2x736;2x737;2x734	3x370
			F2 [243]	18:54:33.96	-30:27:06.5	05/09/13	4x819;2x817	3x390
40	NGC6717	3	F1 [80]	18:55:31.98	-22:45:22.7	06/05/14	619	535
			F2 [125]	18:55:12.41	-22:48:27.0	03/07/14	619	544
			F3 [171]	18:54:51.25	-22:47:57.0	03/07/14	617	544
41	NGC6723	3	F1 [103]	18:59:54.19	-36:43:18.0	03/04/14	666	592
			F2 [148]	18:59:27.49	-36:44:21.9	15/06/14	626	551
			F3 [193]	18:59:06.07	-36:41:59.9	05/07/14	624	551
42	NGC6779	2	F1 [241]	19:16:04.77	+30:12:18.9	13/10/13	731	658
			F2 [333]	19:16:42.17	+30:17:38.2	19/07/14	637	564
43	NGC6791	2	F1 [322]	19:20:53.69	+37:53:04.8	17/08/13	631	559
			F2 [50]	19:21:27.31	+37:46:16.6	26/04/14	638	565
44	NGC6809	2	F1 [262]	19:39:32.79	-30:54:19.4	21/08/14	753	680
			F2 [82]	19:40:26.65	-31:01:26.4	29/03/14	677	604
45	NGC6838	2	F1 [244]	19:53:18.63	+18:48:20.3	23/10/13	723	650
			F2 [75]	19:54:12.48	+18:43:53.9	03/05/14	681	608
46	NGC6934	2	F1 [245]	20:33:44.84	+07:25:55.5	08/10/13	723	650
			F2 [334]	20:34:17.59	+07:30:52.3	18/08/14	644	571
47	NGC6981	2	F1 [289]	20:53:13.45	-12:26:24.9	13/08/13	641	568
			F2 [19]	20:53:51.29	-12:28:39.5	03/08/14	624	551
48	NGC7089	3	F1 [237]	21:32:59.85	+00:48:42.0	18/10/13	717	643
			F2 [281]	21:33:10.93	+00:44:15.0	29/08/13	668	593
			F3 [327]	21:33:29.92	+00:42:39.1	14/08/13	611	534
49	NGC7099	2	F1 [92]	21:40:44.34	-23:15:15.1	08/06/14	656	583
			F2 [182]	21:40:02.30	-23:15:49.0	19/08/14	656	583

variations of the PSF. To mitigate these sources of systematic errors, we derived a set of spatially varying perturbations of the PSF models for each calibrated, non-drizzled (f1c) image. Adopting the procedure presented in [Bellini et al. \(2013\)](#), each image is divided into a grid with a number of cells changing from 2×2 to 5×5 . In each cell, a sub-

set of well measured stars is used to locally adjust the PSF models to the stellar profiles. Using an updated version of [Anderson & King \(2006\)](#) software, in combination with the newly created PSF models, we extracted raw catalogues of stellar positions and magnitudes in each image. We choose the grid refinement (between 2×2 to 5×5) that produces

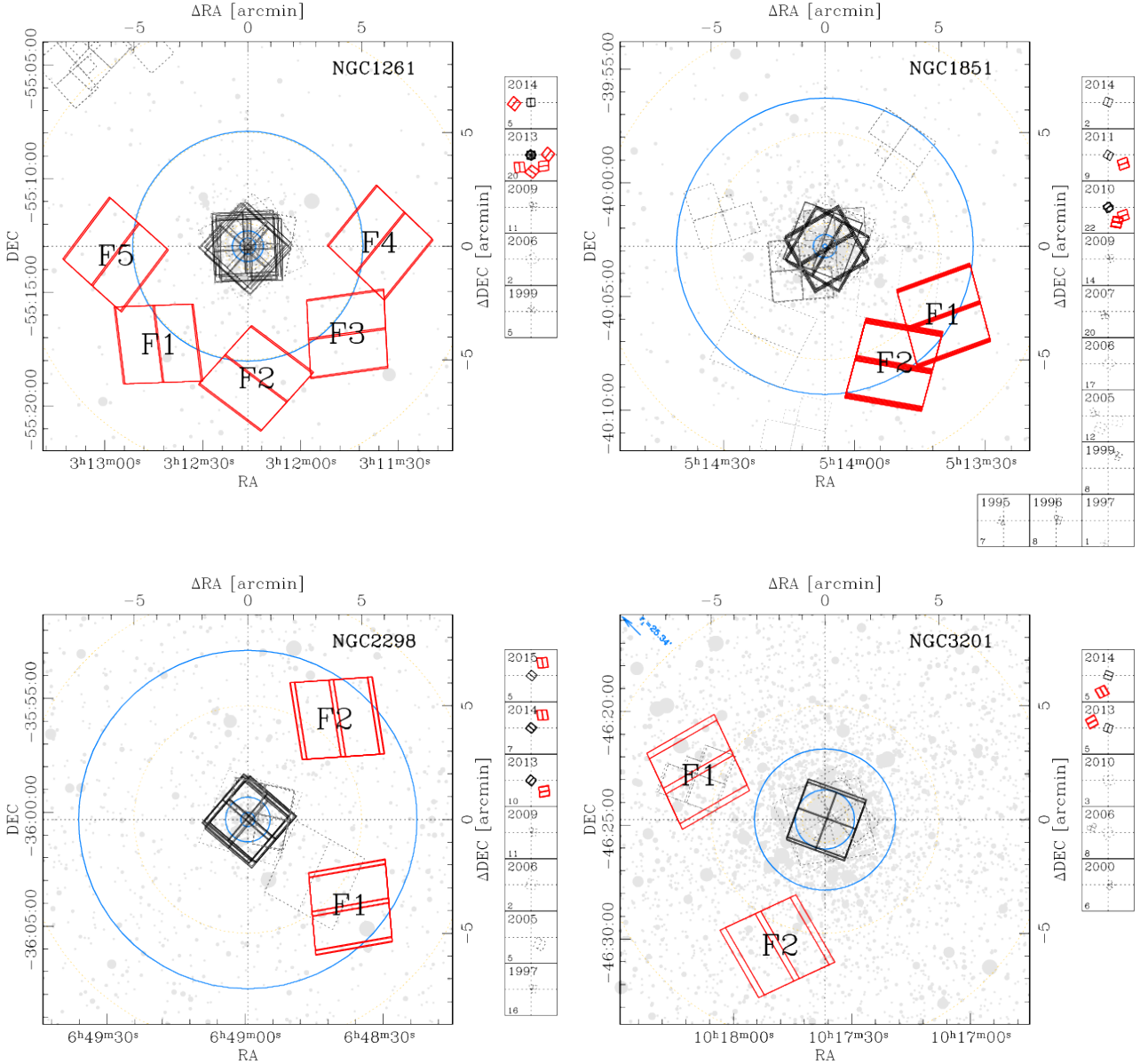


Figure 1. Finding charts for NGC 1261, NGC 1851, NGC 2298 and NGC 3201. Red outlines, represent ACS/WFC parallel observations of GO-13297, black outlines refer to WFC3/UVIS observations. Dark gray, dashed outlines represent archive *HST* observations in the same regions. Footprints are labeled as in Table 1. Observations are subdivided by epoch in the smaller panels. Blue circles mark the position of core radius, half-light radius and tidal radius for each cluster from Harris 1996 (2010 edition). Where the tidal radius could not be included in the image, its value has been indicated in the upper-left corner of the image. Yellow, dashed circles mark the distances of 1, 5 and 10 arcminutes from cluster centres. Gray dots corresponds to 2MASS sources, with brighter sources being larger.

the best results, inspecting the distribution of the quality of fit parameters as a function of magnitude, and taking into account the number of reference stars used to tailor the PSF perturbations in each cell.

Each exposure related to the same field has been subsequently referred to a common reference frame. Since we are mainly interested in the faint, red part of the cluster CMDs, we used the F814W images to construct the reference frames. Catalogues are finally produced using a version of the software presented in Anderson et al. (2008), specifi-

cally tuned for this project. In particular, the `kitchen_sync` routine has been modified in order to work properly with only one image per filter. In addition, the method presented in Gilliland (2004) was applied in order to provide reliable photometry also for saturated stars.

The raw, instrumental magnitudes have been zero-pointed into ACS/WFC Vega-mag photometric system following the prescriptions of Bedin et al. (2005). The zero-points and aperture corrections from 0.5 arcseconds to infinity of Bohlin (2016) have been used.

Especially in the present case, the photometric calibration plays a critical role, and we put strong efforts to precisely evaluate zero-point differences between various observations. Crowding is not a serious problem in the outer cluster regions and high-precision photometric measurements are relatively easy to obtain. But field-to-field zero-point variations must be accounted for to have the external fields of the same cluster on the same photometric scale. The main source of this photometric offsets between catalogues of distinct fields, is related to PSF modelling. The PSF model by construction is normalized to a surface flux of unity within a radius of 10 ACS/WFC pixels (0.5 arcsecond). Only the inner 5×5 -pixel region of sources was used to fit to the PSF model in order to minimize the contaminating impact of nearby neighbors, but any mismatch between the adopted PSF model and the pixels beyond the small square fitting aperture would result in a slight zeropoint shift. The fact that we perturb the library PSFs (above) minimizes this even further. However, the best way to regularize the photometry is empirically: following [Bedin et al. \(2005\)](#) and [Anderson et al. \(2008\)](#), we measured aperture corrections inside this aperture using the calibrated and drizzled (`drc`) images as reference.

These corrections were sufficient to properly take into account the majority of the photometric biases in our catalogues. The obtained values of the aperture correction for an aperture of 0.5 arcseconds are listed in Tables 3 and 4. We maintain the same nomenclature as in [Bedin et al. \(2005\)](#). The aperture correction values, along with their associated uncertainties are also reported in Figure 2. Black dots are referred to F814W observations, red dots to F475W ones. It can be noted that for the majority of cases corrections are small: typically smaller than 0.04 magnitudes, but in the most severe cases, they can reach values as high as 0.15 mag.

Astrometrised, stacked images of each observed field have also been produced for both filters with a 1×1 pixel sampling. These have been created, for each field, combining all overlapping `f1c` images using the same coordinate transformations that define the common reference frames.

Astrometric solutions have been independently derived using the *Gaia* DR1 catalogue as a reference ([Gaia Collaboration et al. 2016](#)). As a consequence, positions are given for Equinox J2000 at epoch 2015. Table 5 reports the precision reached by the new astrometric solution in the fifth column, which is the root mean square error of the offset between *Gaia* positions and those derived, for the same stars, in our astrometrised stacked images. The measured average value is 0.2 pixel, or ~ 10 milliarcseconds. These values are also visualised in Figure 3.

For completeness, we also measure the astrometric precision of the original astrometric solution of `drc` images. The position offset between common sources in the *Gaia* DR1 catalogue and the `drc` images is used to define this quantity. Offset values are referred to RA and DEC distances in image pixels and are reported in columns six and seven of Table 5. The associated errors corresponds to the measured standard deviations of each sample. A visual representation is also given in Figure 4. It can be noted that, in general, offsets are lower than 5 ACS/WFC pixels (0.25 arcseconds), and, in many cases, below 1 pixel, with some notable exceptions.

Table 3. Tabulated $\Delta m_{\text{PSF-AP}(0''.5)}$ values used in the aperture correction

#	CLUSTER	FIELD	$\Delta m_{\text{PSF-AP}(0''.5)}^{\text{F475W}}$ mag	$\Delta m_{\text{PSF-AP}(0''.5)}^{\text{F814W}}$ mag
01	NGC1261	1	$+0.016 \pm 0.006$	-0.017 ± 0.003
		2	$+0.030 \pm 0.005$	-0.021 ± 0.002
		3	$+0.021 \pm 0.005$	-0.013 ± 0.002
		4	$+0.038 \pm 0.005$	$+0.117 \pm 0.005$
		5	$+0.053 \pm 0.006$	-0.020 ± 0.003
02	NGC1851	1+2	-0.008 ± 0.002	-0.004 ± 0.001
03	NGC2298	1	$+0.057 \pm 0.014$	$+0.148 \pm 0.008$
		2	$+0.016 \pm 0.010$	$+0.013 \pm 0.005$
04	NGC3201	1	$+0.022 \pm 0.001$	$+0.001 \pm 0.001$
		2	$+0.023 \pm 0.001$	$+0.035 \pm 0.001$
05	NGC4590	1	-0.003 ± 0.003	$+0.002 \pm 0.002$
		2	0.000 ± 0.003	$+0.039 \pm 0.002$
06	NGC4833	1	$+0.004 \pm 0.002$	$+0.002 \pm 0.001$
		2	$+0.009 \pm 0.001$	-0.008 ± 0.001
07	NGC5024	1	$+0.003 \pm 0.001$	$+0.012 \pm 0.001$
		2	$+0.009 \pm 0.003$	-0.019 ± 0.001
08	NGC5053	1	$+0.012 \pm 0.004$	$+0.001 \pm 0.004$
		2	$+0.003 \pm 0.004$	0.000 ± 0.003
		3	$+0.005 \pm 0.005$	-0.011 ± 0.003
		4	$+0.012 \pm 0.005$	$+0.006 \pm 0.003$
		5	$+0.132 \pm 0.006$	$+0.029 \pm 0.003$
09	NGC5286	1	$+0.036 \pm 0.003$	$+0.019 \pm 0.002$
		2	$+0.031 \pm 0.004$	-0.011 ± 0.001
10	NGC5466	1	$+0.009 \pm 0.003$	-0.011 ± 0.003
		2	$+0.008 \pm 0.003$	-0.009 ± 0.002
11	NGC5897	1	$+0.029 \pm 0.003$	-0.012 ± 0.001
		2	$+0.028 \pm 0.003$	-0.014 ± 0.001
12	NGC5904	1	$+0.011 \pm 0.001$	-0.016 ± 0.001
		2	$+0.003 \pm 0.001$	-0.008 ± 0.001
13	NGC5927	1	$+0.023 \pm 0.002$	$+0.017 \pm 0.001$
		2	$+0.022 \pm 0.002$	-0.003 ± 0.001
14	NGC5986	1	-0.004 ± 0.002	-0.011 ± 0.001
		2	$+0.043 \pm 0.004$	-0.008 ± 0.001
15	NGC6093	1	$+0.090 \pm 0.002$	$+0.136 \pm 0.002$
16	NGC6101	1	$+0.003 \pm 0.003$	$+0.004 \pm 0.002$
		2	$+0.007 \pm 0.003$	-0.012 ± 0.001
		3	$+0.010 \pm 0.004$	$+0.004 \pm 0.002$
		4	$+0.003 \pm 0.002$	-0.014 ± 0.001
		5	$+0.009 \pm 0.002$	-0.001 ± 0.001
17	NGC6121	1	$+0.003 \pm 0.002$	$+0.002 \pm 0.001$
		2	-0.004 ± 0.003	-0.005 ± 0.001
18	NGC6144	1	$+0.030 \pm 0.004$	$+0.027 \pm 0.001$
		2	$+0.013 \pm 0.004$	-0.002 ± 0.001
19	NGC6171	1	$+0.021 \pm 0.002$	-0.007 ± 0.002
		2	$+0.022 \pm 0.002$	$+0.004 \pm 0.002$
20	NGC6218	1	-0.003 ± 0.002	-0.001 ± 0.001
		2	$+0.006 \pm 0.002$	-0.009 ± 0.001
21	NGC6254	1	-0.006 ± 0.002	$+0.002 \pm 0.001$
		2	0.000 ± 0.002	-0.003 ± 0.001
22	NGC6304	1	$+0.010 \pm 0.001$	$+0.036 \pm 0.001$
		2	$+0.012 \pm 0.002$	$+0.016 \pm 0.001$
23	NGC6341	1	$+0.003 \pm 0.002$	-0.026 ± 0.001
		2	$+0.016 \pm 0.002$	-0.013 ± 0.001
24	NGC6352	1	$+0.001 \pm 0.001$	-0.004 ± 0.001
		2	-0.010 ± 0.001	$+0.011 \pm 0.001$

Continued on Tab. 4

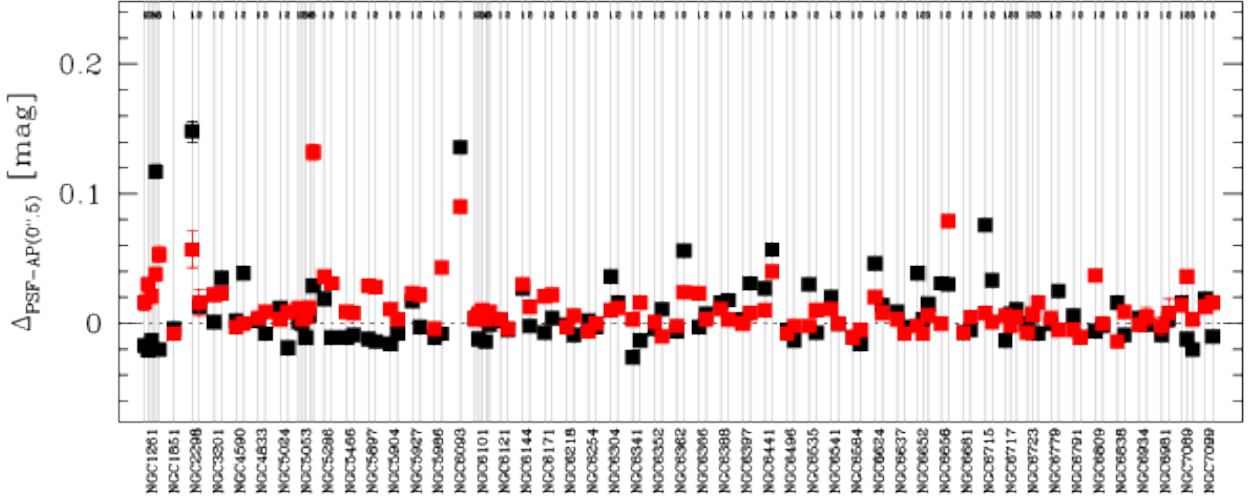


Figure 2. Aperture corrections measured in each field for each cluster. Red squares refer to F475W observations, while black squares refer to F814W ones.

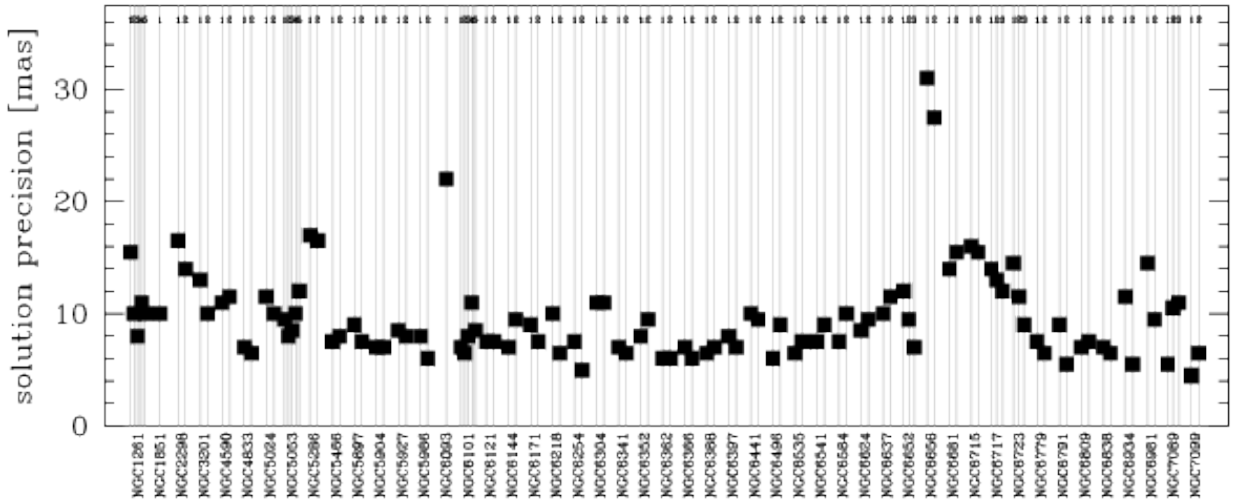


Figure 3. Precision of the redefined astrometric solution for each observed field, see text for details.

3 THE COLOUR-MAGNITUDE DIAGRAMS AND TRICHROMATIC STACKED IMAGES

In Figure 5 we report the CMDs obtained for all 5 fields of NGC 1261. Magnitudes are given both in the instrumental and Vega-mag photometric systems. Dashed lines represent the saturation limit, black dots represent unsaturated stars, saturated stars are represented with crosses. The five CMDs are all merged in the bottom-right panel, where a different colour have been assigned to each different field. In this

case, the instrumental magnitude scale, along with saturation level (dashed line), refer only to Field 1.

The final CMDs for all other targets are presented in Figures A9 - A16. The presented CMDs have been obtained by selecting only high-quality stars, according to quality parameters presented in Anderson et al. (2008). In Section 4 we describe the adopted selection procedure. It is important to mention here that, since in the majority of the cases only one image per filter has been taken, artifact rejection is not an easy task. In order to include faint sources, we have cho-

Table 4. Table 3 (continued)

#	CLUSTER	FIELD	$\Delta m_{\text{PSF-AP}(0''.5)}^{\text{F475W}}$ mag	$\Delta m_{\text{PSF-AP}(0''.5)}^{\text{F814W}}$ mag
25	NGC6362	1	-0.002 ± 0.002	-0.006 ± 0.001
		2	$+0.024 \pm 0.003$	$+0.056 \pm 0.001$
26	NGC6366	1	$+0.023 \pm 0.005$	-0.003 ± 0.001
		2	$+0.003 \pm 0.002$	$+0.007 \pm 0.001$
27	NGC6388	1	$+0.011 \pm 0.001$	$+0.016 \pm 0.001$
		2	$+0.003 \pm 0.001$	$+0.018 \pm 0.001$
28	NGC6397	1	0.000 ± 0.001	$+0.003 \pm 0.001$
		2	$+0.008 \pm 0.002$	$+0.031 \pm 0.001$
29	NGC6441	1	$+0.010 \pm 0.001$	$+0.027 \pm 0.001$
		2	$+0.040 \pm 0.001$	$+0.057 \pm 0.001$
30	NGC6496	1	-0.008 ± 0.002	-0.005 ± 0.001
		2	-0.002 ± 0.001	-0.013 ± 0.001
31	NGC6535	1	-0.002 ± 0.002	$+0.030 \pm 0.001$
		2	$+0.010 \pm 0.003$	-0.007 ± 0.001
32	NGC6541	1	$+0.011 \pm 0.001$	$+0.020 \pm 0.001$
		2	0.000 ± 0.002	0.000 ± 0.001
33	NGC6584	1	-0.011 ± 0.003	-0.011 ± 0.001
		2	-0.005 ± 0.004	-0.016 ± 0.001
34	NGC6624	1	$+0.020 \pm 0.001$	$+0.046 \pm 0.001$
		2	$+0.008 \pm 0.001$	$+0.014 \pm 0.001$
35	NGC6637	1	$+0.003 \pm 0.001$	$+0.009 \pm 0.001$
		2	-0.008 ± 0.001	-0.003 ± 0.001
36	NGC6652	1	-0.002 ± 0.002	$+0.039 \pm 0.001$
		2	-0.008 ± 0.002	$+0.003 \pm 0.001$
		3	$+0.006 \pm 0.001$	$+0.015 \pm 0.001$
37	NGC6656	1	0.000 ± 0.001	$+0.031 \pm 0.001$
		2	$+0.079 \pm 0.001$	$+0.030 \pm 0.001$
38	NGC6681	1	-0.007 ± 0.001	-0.007 ± 0.001
		2	$+0.005 \pm 0.001$	-0.005 ± 0.001
39	NGC6715	1	$+0.008 \pm 0.001$	$+0.076 \pm 0.001$
		2	$+0.001 \pm 0.001$	$+0.033 \pm 0.001$
40	NGC6717	1	$+0.006 \pm 0.002$	-0.013 ± 0.001
		2	-0.002 ± 0.002	$+0.007 \pm 0.001$
		3	$+0.005 \pm 0.001$	$+0.011 \pm 0.001$
41	NGC6723	1	-0.007 ± 0.003	0.000 ± 0.001
		2	$+0.007 \pm 0.002$	-0.007 ± 0.001
		3	$+0.016 \pm 0.003$	-0.008 ± 0.001
42	NGC6779	1	$+0.004 \pm 0.003$	0.000 ± 0.002
		2	-0.005 ± 0.002	$+0.025 \pm 0.002$
43	NGC6791	1	-0.005 ± 0.004	$+0.006 \pm 0.002$
		2	-0.011 ± 0.003	-0.011 ± 0.001
44	NGC6809	1	$+0.037 \pm 0.002$	-0.006 ± 0.001
		2	0.000 ± 0.001	-0.002 ± 0.001
45	NGC6838	1	-0.014 ± 0.002	$+0.016 \pm 0.001$
		2	$+0.009 \pm 0.002$	-0.009 ± 0.001
46	NGC6934	1	-0.001 ± 0.005	$+0.004 \pm 0.002$
		2	$+0.005 \pm 0.007$	-0.001 ± 0.003
47	NGC6981	1	-0.002 ± 0.007	-0.009 ± 0.003
		2	$+0.008 \pm 0.011$	$+0.003 \pm 0.005$
48	NGC7089	1	$+0.014 \pm 0.003$	$+0.016 \pm 0.001$
		2	$+0.036 \pm 0.002$	-0.012 ± 0.001
		3	$+0.003 \pm 0.002$	-0.020 ± 0.001
49	NGC7099	1	$+0.013 \pm 0.003$	$+0.019 \pm 0.002$
		2	$+0.016 \pm 0.004$	-0.010 ± 0.002

Table 5. Precision reached with the re-derived astrometric solution using *Gaia* catalogues; for completeness we report the number of reference stars used. We also provide measures of the accuracy of the original STScI astrometric solution in the form of differences between RA and DEC.

#	CLUSTER	F	stars	precision mas	Δ RA WFC px	Δ DEC WFC px
01	NGC1261	1	32	15.5	1.66 ± 0.34	-4.50 ± 0.16
		2	41	10.0	-1.89 ± 0.08	4.31 ± 0.21
		3	37	8.0	-0.51 ± 0.06	1.61 ± 0.18
		4	36	11.0	-0.50 ± 0.14	1.03 ± 0.31
		5	46	10.0	0.07 ± 0.05	-4.81 ± 0.19
02	NGC1851	1+2232	10.0	3.54 ± 0.20	-4.25 ± 0.19	
03	NGC2298	1	79	16.5	-0.17 ± 0.04	5.62 ± 0.24
		2	53	14.0	-0.11 ± 0.06	-1.37 ± 0.25
04	NGC3201	1	635	13.0	0.14 ± 0.32	-0.57 ± 0.23
		2	653	10.0	4.33 ± 0.33	8.39 ± 0.20
05	NGC4590	1	110	11.0	-0.78 ± 0.10	4.90 ± 0.15
		2	111	11.5	-0.12 ± 0.04	-3.86 ± 0.17
06	NGC4833	1	492	7.0	-3.53 ± 0.35	6.86 ± 0.22
		2	570	6.5	1.75 ± 0.15	-0.02 ± 0.20
07	NGC5024	1	173	11.5	-0.14 ± 0.23	3.09 ± 0.20
		2	142	10.0	-45.45 ± 0.77	1.35 ± 0.18
08	NGC5053	1	44	9.5	0.72 ± 0.16	-0.62 ± 0.16
		2	41	8.0	-0.07 ± 0.15	-1.86 ± 0.18
		3	38	8.5	0.22 ± 0.13	0.29 ± 0.23
		4	42	10.0	0.43 ± 0.09	0.23 ± 0.19
		5	52	12.0	0.57 ± 0.16	-0.65 ± 0.16
09	NGC5286	1	215	17.0	1.63 ± 0.20	1.85 ± 0.25
		2	217	16.5	1.61 ± 0.20	1.10 ± 0.21
10	NGC5466	1	56	7.5	-0.13 ± 0.27	1.37 ± 0.12
		2	72	8.0	-0.79 ± 0.29	-2.22 ± 0.20
11	NGC5897	1	164	9.0	0.12 ± 0.22	-0.37 ± 0.20
		2	154	7.5	2.58 ± 0.17	-2.51 ± 0.18
12	NGC5904	1	579	7.0	-1.29 ± 0.19	-2.69 ± 0.15
		2	630	7.0	-0.16 ± 0.15	-1.08 ± 0.22
13	NGC5927	1	848	8.5	3.65 ± 0.30	-0.38 ± 0.20
		2	985	8.0	-9.20 ± 0.35	11.91 ± 0.21
14	NGC5986	1	278	8.0	-0.54 ± 0.30	1.36 ± 0.22
		2	268	6.0	-6.46 ± 0.26	4.12 ± 0.18
15	NGC6093	1	236	22.0	1.81 ± 0.19	-4.47 ± 0.20
16	NGC6101	1	235	7.0	-1.85 ± 0.76	1.09 ± 0.21
		2	232	6.5	-0.80 ± 0.61	2.90 ± 0.20
		3	229	8.0	-15.82 ± 0.73	0.55 ± 0.25
		4	263	11.0	-1.83 ± 0.89	-0.52 ± 0.27
		5	204	8.5	12.13 ± 0.85	-3.52 ± 0.24
17	NGC6121	1	633	7.5	-4.81 ± 0.37	7.07 ± 0.23
		2	649	7.5	-0.69 ± 0.14	1.90 ± 0.22
18	NGC6144	1	147	7.0	-4.48 ± 0.18	-0.10 ± 0.19
		2	147	9.5	-3.09 ± 0.15	-0.76 ± 0.20
19	NGC6171	1	172	9.0	4.44 ± 0.20	-2.36 ± 0.16
		2	196	7.5	-3.26 ± 0.19	-1.51 ± 0.21
20	NGC6218	1	300	10.0	0.40 ± 0.07	-4.05 ± 0.17
		2	362	6.5	-0.72 ± 0.09	0.13 ± 0.19
21	NGC6254	1	525	7.5	-0.94 ± 0.11	2.02 ± 0.20
		2	507	5.0	-0.08 ± 0.12	-0.52 ± 0.18
22	NGC6304	1	1021	11.0	0.00 ± 0.09	7.29 ± 0.22
		2	1137	11.0	-2.63 ± 0.15	3.66 ± 0.28
23	NGC6341	1	272	7.0	3.31 ± 0.13	-1.46 ± 0.17
		2	276	6.5	1.30 ± 0.16	2.01 ± 0.14

continued on Table 6

Table 6. Table 5 (continued)

#	CLUSTER	F	stars	precision mas	ΔRA WFC px	ΔDEC WFC px
24	NGC6352	1	676	8.0	0.44 ± 0.09	6.24 ± 0.18
		2	658	9.5	0.20 ± 0.11	0.84 ± 0.21
25	NGC6362	1	399	6.0	-1.98 ± 0.18	-1.19 ± 0.20
		2	412	6.0	-0.15 ± 0.23	2.51 ± 0.17
26	NGC6366	1	265	7.0	1.07 ± 0.11	-4.03 ± 0.22
		2	263	6.0	2.89 ± 0.19	4.66 ± 0.18
27	NGC6388	1	812	6.5	1.68 ± 0.24	4.01 ± 0.26
		2	873	7.0	-0.86 ± 0.22	5.67 ± 0.22
28	NGC6397	1	605	8.0	16.46 ± 0.47	12.42 ± 0.26
		2	602	7.0	-4.15 ± 0.33	4.79 ± 0.30
29	NGC6441	1	1075	10.0	34.98 ± 0.54	-3.77 ± 0.26
		2	1114	9.5	4.46 ± 0.31	3.80 ± 0.27
30	NGC6496	1	482	6.0	1.85 ± 0.30	7.03 ± 0.21
		2	525	9.0	8.00 ± 0.28	1.65 ± 0.22
31	NGC6535	1	304	6.5	-4.97 ± 0.19	0.75 ± 0.18
		2	275	7.5	-1.78 ± 0.18	-9.16 ± 0.20
32	NGC6541	1	385	7.5	-11.12 ± 0.28	7.28 ± 0.23
		2	481	9.0	-7.23 ± 0.32	7.72 ± 0.22
33	NGC6584	1	119	7.5	1.82 ± 0.19	6.15 ± 0.24
		2	141	10.0	2.67 ± 0.14	2.71 ± 0.25
34	NGC6624	1	360	8.5	0.83 ± 0.12	1.93 ± 0.23
		2	774	9.5	0.61 ± 0.15	6.08 ± 0.21
35	NGC6637	1	620	10.0	-3.66 ± 0.20	1.83 ± 0.25
		2	615	11.5	-2.54 ± 0.23	-0.80 ± 0.29
36	NGC6652	1	608	12.0	0.35 ± 0.09	5.17 ± 0.26
		2	624	9.5	-0.06 ± 0.06	2.40 ± 0.25
		3	682	7.0	0.49 ± 0.15	5.78 ± 0.21
37	NGC6656	1	734	31.0	-1.20 ± 0.21	3.03 ± 0.25
		2	1052	27.5	1.21 ± 0.30	6.93 ± 0.31
38	NGC6681	1	450	14.0	-4.20 ± 0.25	1.76 ± 0.29
		2	385	15.5	-2.37 ± 0.20	1.75 ± 0.32
39	NGC6715	1	484	16.0	-0.69 ± 0.25	-4.67 ± 0.28
		2	505	15.5	3.28 ± 0.18	-1.79 ± 0.27
40	NGC6717	1	439	14.0	3.48 ± 0.21	0.07 ± 0.30
		2	406	13.0	0.49 ± 0.20	1.11 ± 0.28
		3	445	12.0	0.11 ± 0.18	4.99 ± 0.26
41	NGC6723	1	256	14.5	0.14 ± 0.20	0.95 ± 0.30
		2	144	11.5	-0.25 ± 0.19	4.59 ± 0.22
		3	111	9.0	-0.33 ± 0.16	3.99 ± 0.18
42	NGC6779	1	345	7.5	0.86 ± 0.07	1.07 ± 0.21
		2	333	6.5	3.24 ± 0.16	-8.92 ± 0.19
43	NGC6791	1	288	9.0	-1.92 ± 0.26	-7.50 ± 0.21
		2	274	5.5	-4.98 ± 0.25	-6.18 ± 0.21
44	NGC6809	1	584	7.0	-1.58 ± 0.19	0.99 ± 0.22
		2	590	7.5	-9.19 ± 0.21	-0.68 ± 0.23
45	NGC6838	1	816	7.0	-8.81 ± 0.24	-12.24 ± 0.22
		2	800	6.5	-3.96 ± 0.22	-8.28 ± 0.21
46	NGC6934	1	87	11.5	3.41 ± 0.20	2.62 ± 0.24
		2	84	5.5	1.41 ± 0.10	-12.00 ± 0.17
47	NGC6981	1	31	14.5	1.29 ± 0.26	-9.37 ± 0.19
		2	27	9.5	1.73 ± 0.23	-8.07 ± 0.23
48	NGC7089	1	92	5.5	-0.55 ± 0.12	-6.84 ± 0.15
		2	77	10.5	2.52 ± 0.15	-1.40 ± 0.18
		3	82	11.0	1.85 ± 0.12	-0.54 ± 0.20
49	NGC7099	1	79	4.5	0.93 ± 0.08	-0.89 ± 0.17
		2	89	6.5	0.66 ± 0.08	1.75 ± 0.21

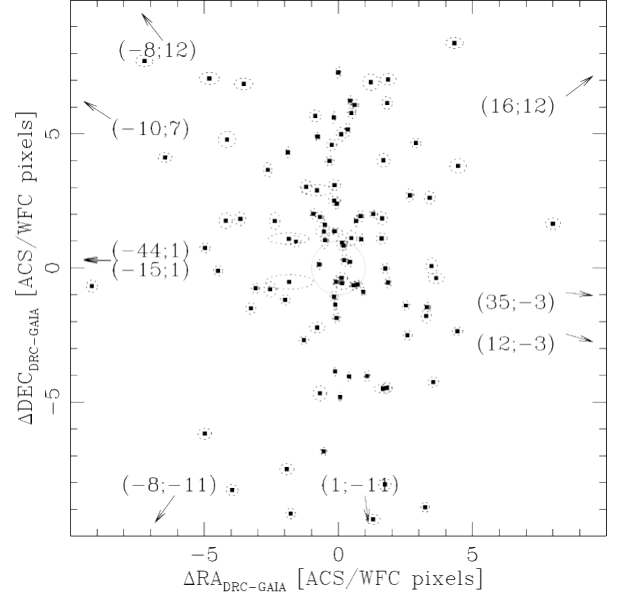


Figure 4. Offsets between star positions obtained using the original STScI astrometric solution (header of *drc* images) and *Gaia* ones. Points represent single fields; the semi-axes of each ellipse have length equal to the measured standard deviation. The gray circle represents an offset of 1 ACS/WFC pixel, which corresponds to ~ 0.05 arcseconds. Some points falls outside the used limits; we indicate their position along the edges of the figure, the arrows point in their direction.

sen not to limit in flux our raw catalogues. We nonetheless restricted the detections only to those sources observed in at least one F814W and one F475W image simultaneously, with positions in the common reference frame consistent within 0.8 pixels.

No rejection of foreground/background contamination has been performed, nor any correction for differential reddening. The homogeneity of the data guarantees very similar results in every case. Nonetheless, it is out of the scope of the present work to characterize in detail the obtained results, which require taking into consideration several issues. For example, the number density of cluster members present in the observed fields depends on the properties of each GC: in some cases, especially for bulge clusters, or those that appear projected in this dense Galactic region, it is difficult to identify the cluster sequence. We recall that another interesting application of the present data is the study of the stellar populations, external to the clusters, that contaminate the observed fields. In particular, for at least 6 GCs, namely NGC 6624, NGC 6637, NGC 6652, NGC 6681, NGC 6715 and NGC 6809, traces of the Sagittarius Stream are visible in the obtained CMDs (Siegel et al. 2011).

As an additional tool to explore and characterize observations, we have created colour images of each observed field, combining the astrometrised stacked images: an example is shown in Figure 6. The F814W stacked images have been associated with red channel while the F475W images are associated to the blue channel. The images associated

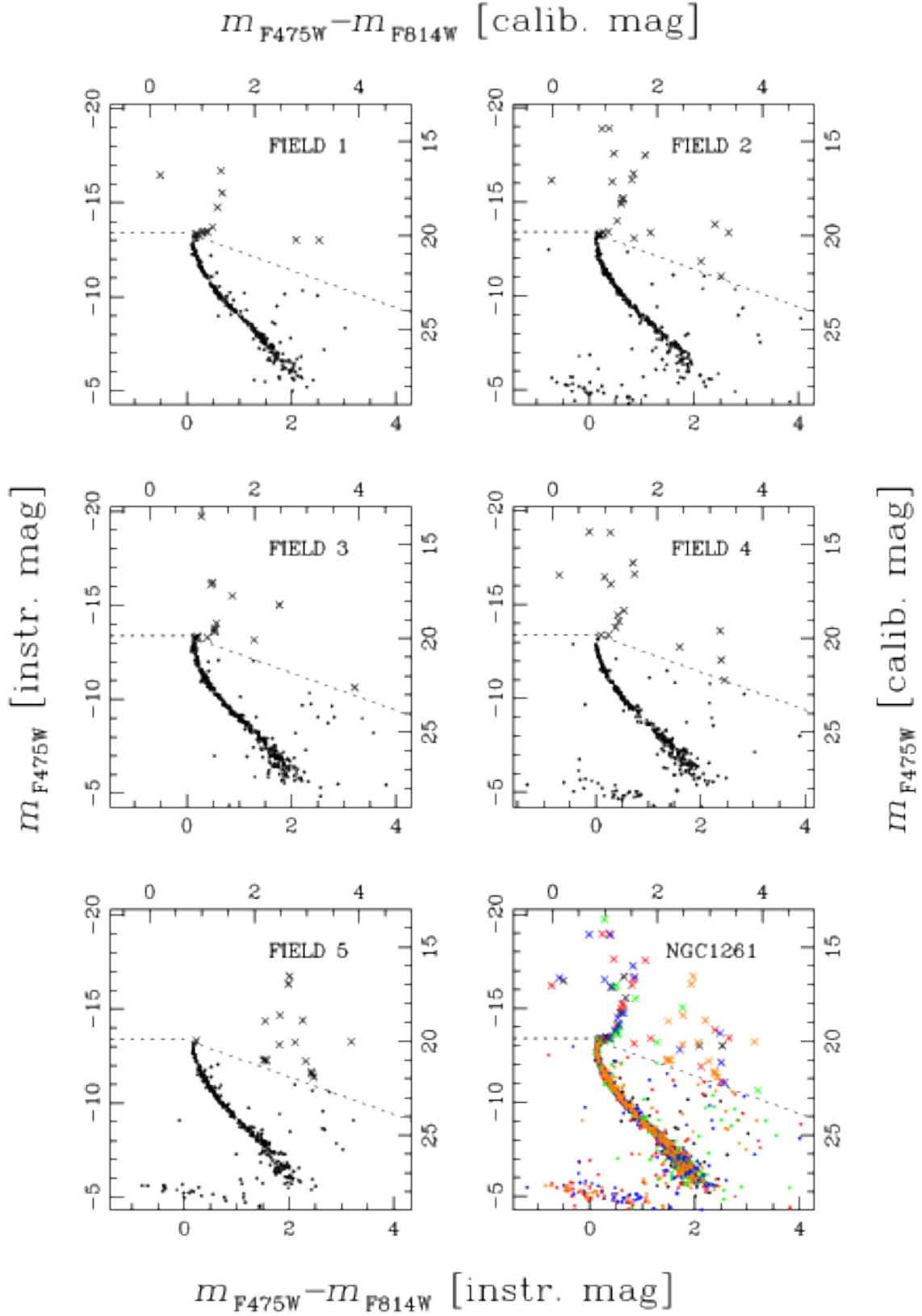


Figure 5. CMDs of the parallel fields of NGC 1261. Both instrumental and calibrated magnitude scales are shown. Dashed lines represent the saturation levels. Saturated stars are marked with crosses. The bottom-right panel collects all the stars present in all the five fields. Stars are here colour-coded as follows. Black dots represent stars measured in F1, red dots stars of F2, green dots stars of F3, blue dots stars of F4, and orange dots represent stars measured in F5. The instrumental magnitude scale and the saturation limit refer to F1 only.

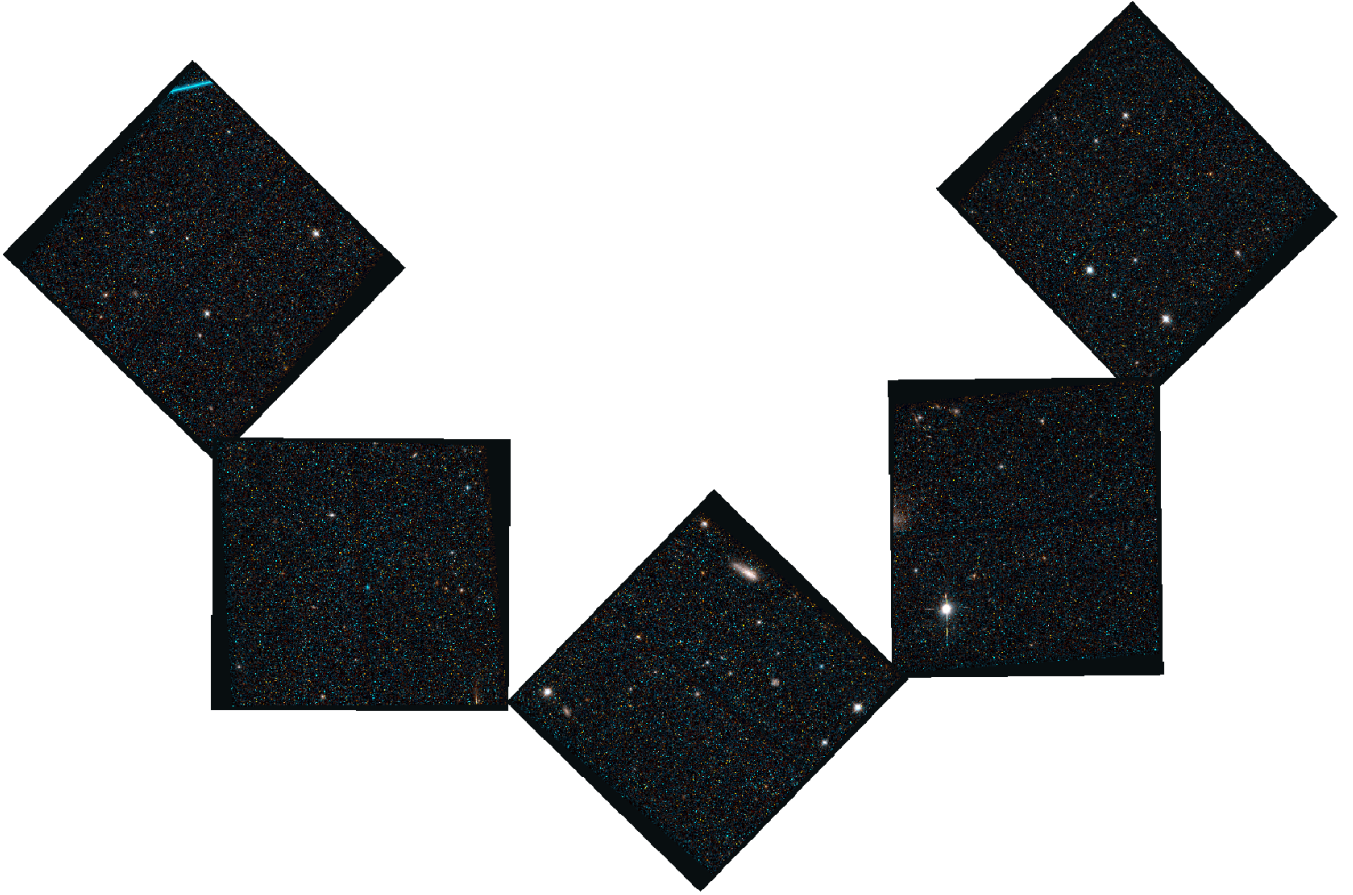


Figure 6. Mosaic of all trichromatic images created for NGC 1261; see text for details.

to the green channel have been obtained as a result of a 3:1 weighted mean of F475W and F814W counts respectively.

4 SELECTION OF WELL-MEASURED STARS

This section describes the procedure adopted to reject spurious or poorly measured sources in the catalogues and to obtain a sample of bona-fide stellar sources. In this example we refer to the catalogue associated to Field 1 of NGC 6121 (M4). The V3 PA is 272 degrees and, for this field, 2 images were collected, one in F814W, and the other in F475W (666 and 739 seconds respectively).

For the selection, we have adopted a procedure similar to that described in Milone et al. (2012), defining limits in both q and o (quality) parameters. In addition, we also made use of the *RADXS* parameter (Bedin et al. 2008, Bedin et al. 2009, Bedin et al. 2010).

As shown in the lower left panels of Figure 7, the q parameter displays a characteristic trend with magnitude. This parameter is defined as the absolute value of the subtraction between the PSF model and the spatial distribution of light of a particular detection in the image, inside the fitting radius. For a perfectly modeled source, the q parameter assumes value 0.

The o parameter quantifies the amount of light that falls on the aperture used for PSF fitting, due to neighboring sources (Anderson et al. 2008). Unlike the q parameter, it does not show a clear trend with magnitude (middle-left panels of Figure 7), for this reason we have used a fixed limit (Milone et al. 2012).

Finally, the *RADXS* parameter is related to the spatial extent of the sources, and it is used to distinguish between point sources and extended sources. It is defined as the flux in excess of that predicted from the PSF fitting just outside the core of each source (Bedin et al. 2008). Positive values are expected for extended objects, while negative values indicate detections that are sharper than stellar. The introduction of this parameter in the selection process for the present case is particularly necessary: since only one image per filter is available for most cases, spurious detections due to cosmic rays are present in the catalogues. Moreover, these observations cover the external regions of GCs, where the stellar density is not as high as in the central regions. The observed fields are thus relatively populated by extra-galactic, non-stellar objects.

We started by taking a more stringent limit in position-consistency for each source. We selected only sources with an rms error in position less than 0.3 pixel. We adopted

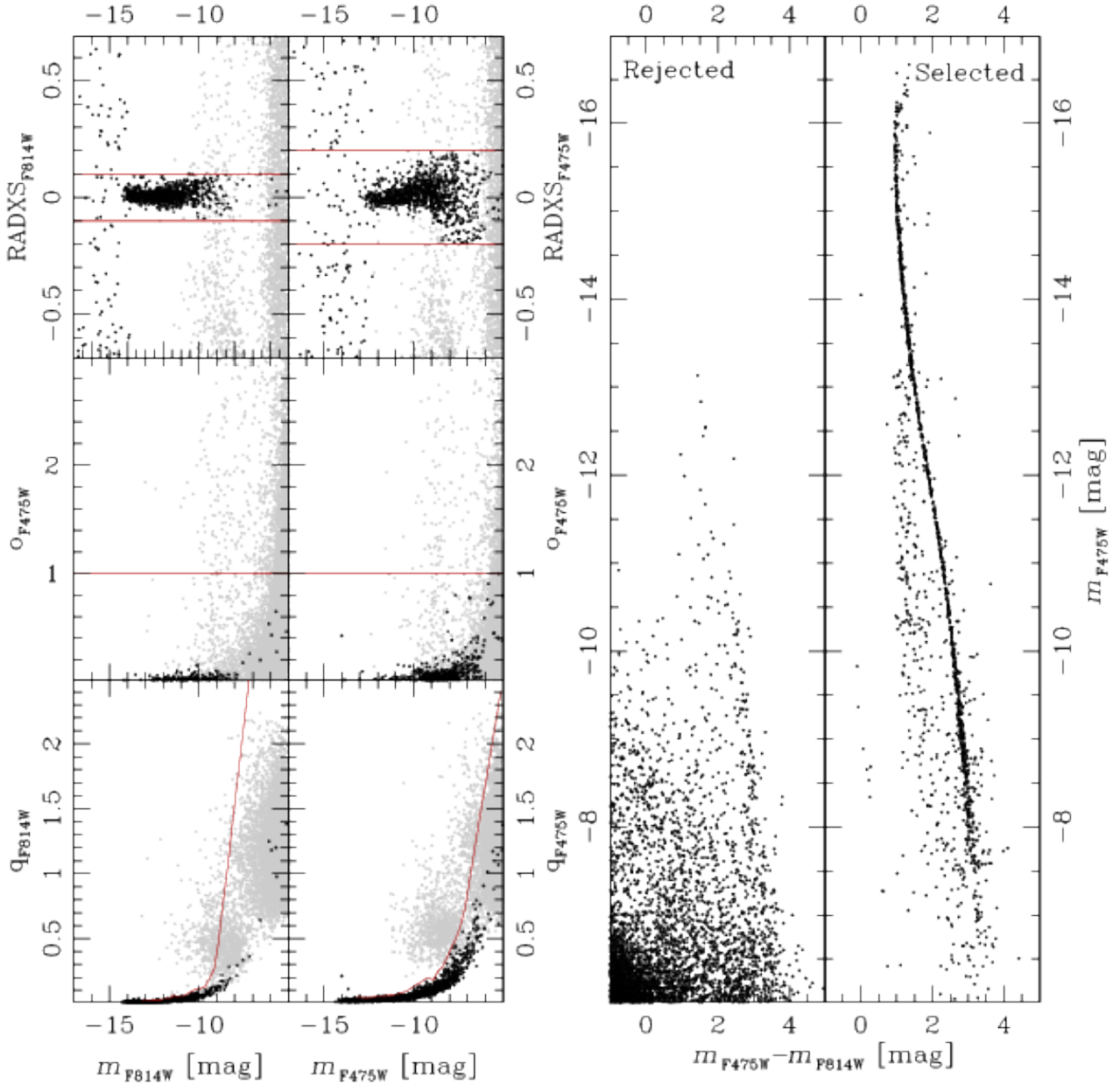


Figure 7. Selection procedure for Field 1 of NGC 6121. Left panels: black points mark the stars that were selected as well-measured. Red lines mark the limits chosen for the q , o and $RADXS$ parameters. Second panel from right: CMD of rejected sources. Right panel: CMD with only sources that survived the selection. All plots refer to instrumental magnitudes.

fixed limits in the o and $RADXS$ parameters for both filters simultaneously. Finally, we measured, for the sources that survived this first selection, the median trend in the plane defined by magnitude and q parameter values. In this way, we removed from the sample non-stellar and poorly-measured sources, while not a priori losing faint sources. Red lines in the left panels of Figure 7 represent the limits used for the case of Field 1 of NGC 6121 (M4). Black points represent sources that passed the selection process.

The CMD corresponding to rejected sources (grey dots in the left panels) is shown in the second panel from the right.

The resulting CMD is shown in the right panel of Figure 7. Note how the cleaning process allows the clear detection of the white-dwarf cooling sequence. Saturated stars have been excluded from the selection procedure, but their fluxes have been recovered using the procedure described in Gilliland (2004).

5 RELEASED ELECTRONIC MATERIAL

We release, for each ACS/WFC parallel field, the astrometric and photometric catalogues and trichromatic astrometrised stacked images. All the released material will be available for download at the website of the Exoplanets & Stellar Populations Group of the Università degli Studi di Padova¹.

Table 7 shows the first ten rows of the catalogue produced for Field 1 of NGC 6121. The content of each column is explained in detail in Table 8. The parameters *wi* and *wb* are the same as in Anderson et al. (2008). They are records that represent the level of saturation of each source in F814W and F475W images respectively. The last column includes the results of the selection of well-measured stars presented in Section 4.

Note that for many stars, we report a magnitude rms error of 9.900. This is because the routine empirically determines errors based on multiple observations in each filter. When there is only one observation per filter, the error is given a high default value.

6 SUMMARY AND CONCLUSIONS

In the context of the *Hubble Space Telescope* UV Legacy Survey Treasury program of Galactic Globular Clusters (GO-13297; PI: Piotto, Paper I), we are releasing the photometric catalogues relative to the ACS/WFC parallel observations. They represent the first *HST* photometric survey of external regions of Galactic GCs and consist of 109 distinct stellar fields of 49 targets: 48 GCs and one open cluster, NGC 6791.

In the majority of cases, only two images per field were taken, one in F814W and one in F475W, centred at about 6.5 arcminutes from cluster centre. Exposure times were selected in order to obtain reliable photometry of the main sequence of target GCs.

These observations complement the WFC3 observations of the central regions of the surveyed GCs, and represent valuable tools for different investigations as outlined in Paper I. These data represent a first epoch for future studies aimed at proper motions measurements in these regions. Even without proper motions, these catalogues are suitable to various interesting studies such as measurements of mass functions and binaries fractions in external regions of GCs. Furthermore, crowding is not an issue in these external cluster fields, as a result, this database could be also used as an input list for spectroscopic follow-up, for example for precise chemical tagging of cluster members.

ACKNOWLEDGEMENTS

We thank the anonymous referee for his careful revision that improved the quality of the present manuscript. M.S., A.A. and G.P. acknowledge support from the Spanish Ministry of Economy and Competitiveness (MINECO) under grant AYA2013-42781. M.S. and A.A. acknowledge support from the Instituto de Astrofísica de Canarias (IAC) under grant 309403. G.P. acknowledges partial support by

the Università degli Studi di Padova Progetto di Ateneo CPDA141214 “Towards understanding complex star formation in Galactic globular clusters” and by INAF under the program PRIN-INAF2014. A.P.M. acknowledges support by the Australian Research Council through Discovery Early Career Researcher Award DE150101816 and by the ERC-StG 2016 716082 project ‘GALFOR’ funded by the European Research Council. This work has made use of data from the European Space Agency (ESA) mission *Gaia* (<http://www.cosmos.esa.int/gaia>), processed by the *Gaia* Data Processing and Analysis Consortium (DPAC, <http://www.cosmos.esa.int/web/gaia/dpac/consortium>). Funding for the DPAC has been provided by national institutions, in particular the institutions participating in the *Gaia* Multilateral Agreement.

REFERENCES

- Anderson, A. J. 1997, Ph.D. Thesis, 1153
 Anderson, J., & King, I. R. 2006, Instrument Science Report ACS 2006-01, 34 pages,
 Anderson, J., Sarajedini, A., Bedin, L. R., et al. 2008, *AJ*, 135, 2055
 Anderson, J., & Bedin, L. R. 2010, *PASP*, 122, 1035
 Bedin, L. R., Piotto, G., Anderson, J., et al. 2004, *ApJ*, 605, L125
 Bedin, L. R., Cassisi, S., Castelli, F., et al. 2005, *MNRAS*, 357, 1038
 Bedin, L. R., King, I. R., Anderson, J., et al. 2008, *ApJ*, 678, 1279-1291
 Bedin, L. R., Salaris, M., Piotto, G., et al. 2009, *ApJ*, 697, 965
 Bedin, L. R., Salaris, M., King, I. R., et al. 2010, *ApJ*, 708, L32
 Bellini, A., Piotto, G., Bedin, L. R., et al. 2009, *A&A*, 507, 1393
 Bellini, A., Bedin, L. R., Piotto, G., et al. 2010, *AJ*, 140, 631
 Bellini, A., Anderson, J., Salaris, M., et al. 2013, *ApJ*, 769, L32
 Bohlin, R. C. 2016, *AJ*, 152, 60
 Carretta, E., Bragaglia, A., Gratton, R. G., et al. 2009a, *A&A*, 505, 117
 Carretta, E., Bragaglia, A., Gratton, R., & Lucatello, S. 2009b, *A&A*, 505, 139
 Cassisi, S., Salaris, M., Pietrinferni, A., & Hyder, D. 2017, *MNRAS*, 464, 2341
 D’Ercole, A., Vesperini, E., D’Antona, F., McMillan, S. L. W., & Recchi, S. 2008, *MNRAS*, 391, 825
 Gaia Collaboration, Brown, A. G. A., Vallenari, A., et al. 2016, *A&A*, 595, A2
 Gilliland, R. L. 2004, Instrument Science Report ACS 2004-01, 18 pages,
 Gratton, R., Sneden, C., & Carretta, E. 2004, *ARA&A*, 42, 385
 Gratton, R. G., Carretta, E., & Bragaglia, A. 2012, *A&ARv*, 20, 50
 Harris, W. E. 1996, *AJ*, 112, 1487
 Kraft, R. P. 1994, *PASP*, 106, 553
 Lee, Y.-W., Joo, J.-M., Sohn, Y.-J., et al. 1999, *Nature*, 402, 55
 Marino, A. F., Villanova, S., Piotto, G., et al. 2008, *A&A*, 490, 625
 Milone, A. P., Bedin, L. R., Piotto, G., et al. 2008, *ApJ*, 673, 241-250
 Milone, A. P., Piotto, G., Bedin, L. R., et al. 2012, *A&A*, 540, A16
 Milone, A. P., Piotto, G., Renzini, A., et al. 2017, *MNRAS*, 464, 3636
 Pancino, E., Ferraro, F. R., Bellazzini, M., Piotto, G., & Zoccali, M. 2000, *ApJ*, 534, L83
 Paust, N. E. Q., Reid, I. N., Piotto, G., et al. 2010, *AJ*, 139, 476

¹ <http://groups.dfa.unipd.it/ESPG/treasury.php>

Table 7. First ten rows extracted from the catalogue referring to Field 1 of NGC 6121 (M4). A detailed description of each column is given in Table 8.

#id	ra(2015)	dec(2015)	x	dx	y	dy	F814W	di	F475W	db	qi	qb	oi	ob	RADXS _i	RADXS _b	ni	nb	wi	wb	good
00000001	245.78962440	-26.47823845	549.416	0.353	688.174	0.224	28.832	9.900	27.078	9.900	1.620	0.760	1.526	0.115	-0.9900	-0.9157	1	1	1	1	0
00000002	245.78961100	-26.47812901	557.336	0.452	687.260	0.382	26.948	9.900	29.764	9.900	1.384	1.274	0.772	9.900	6.2647	-0.9900	1	1	1	1	0
00000003	245.78968050	-26.47823281	549.844	0.632	691.807	0.152	27.164	9.900	28.433	9.900	1.285	1.234	0.179	0.998	-0.9900	-0.9900	1	1	1	1	0
00000004	245.78969050	-26.47817087	554.332	0.391	692.424	0.136	27.335	9.900	30.545	9.900	1.229	1.715	1.014	2.384	0.9430	-0.9900	1	1	1	1	0
00000005	245.78969230	-26.47815496	555.485	0.426	692.537	0.076	27.109	9.900	29.691	9.900	1.189	1.274	0.404	9.900	2.2225	-0.9900	1	1	1	1	0
00000006	245.78973530	-26.47813294	557.094	0.032	695.317	0.263	28.421	9.900	28.038	9.900	1.204	1.009	3.708	0.336	5.6081	-0.9900	1	1	1	1	0
00000007	245.78971500	-26.47807749	561.102	0.068	693.975	0.088	27.108	9.900	28.184	9.900	1.187	0.948	0.787	0.228	1.0828	-0.9900	1	1	1	1	0
00000008	245.78970010	-26.47806742	561.826	0.001	693.008	0.354	26.711	9.900	30.436	9.900	1.154	1.722	0.354	2.059	-0.9900	-0.9900	1	1	1	1	0
00000009	245.78977530	-26.47818364	553.437	0.442	697.928	0.434	27.300	9.900	28.887	9.900	1.330	1.371	0.459	1.208	-0.7255	9.9900	1	1	1	1	0
00000010	245.79005820	-26.47833427	542.628	0.483	716.320	0.322	26.991	9.900	28.863	9.900	1.025	1.193	0.699	5.580	1.8430	1.1484	1	1	1	1	0

Table 8. Information provided by each catalogue.

Col.	Name	Explanation
01	id	ID number for each star
02	ra	Right Ascension for each star (in deg, epoch 2015)
03	dec	Declination for each star (in deg, epoch 2015)
04	x	x position of each star on the reference frame (in pixels)
05	dx	rms errors associated to x position (in pixels)
06	y	y position of each star on the reference frame (in pixels)
07	dy	rms errors associated to y position (in pixels)
08	F814W	F814W magnitude calibrated into Vega-mag system
09	di	rms errors associated to F814W magnitude
10	F475W	F475W magnitude calibrated into Vega-mag system
11	db	rms errors associated to F475W magnitude
12	qi	q parameter for F814W magnitudes
13	qb	q parameter for F475W magnitudes
14	oi	o parameter for F814W magnitudes
15	ob	o parameter for F475W magnitudes
16	RADXS _i	<i>RADXS</i> parameter for F814W
17	RADXS _b	<i>RADXS</i> parameter for F475W
18	ni	number of F814W images the source has been detected in
19	nb	number of F475W images the source has been detected in
20	wi	source of F814W photometry 1: unsaturated in deep; 2: unsaturated in short; 3: saturated in short; 4: saturated in deep;
21	wb	source of F475W photometry (same as wi)
22	good	the source has passed the selection process

- Piotto, G., King, I. R., Djorgovski, S. G., et al. 2002, *A&A*, 391, 945
- Piotto, G., Bedin, L. R., Anderson, J., et al. 2007, *ApJ*, 661, L53
- Piotto, G., Milone, A. P., Bedin, L. R., et al. 2015, *AJ*, 149, 91
- Rosenberg, A., Piotto, G., Saviane, I., & Aparicio, A. 2000 a, *A&AS*, 144, 5
- Rosenberg, A., Aparicio, A., Saviane, I., & Piotto, G. 2000 b, *A&AS*, 145, 451
- Sarajedini, A., Bedin, L. R., Chaboyer, B., et al. 2007, *AJ*, 133, 1658
- Sbordone, L., Salaris, M., Weiss, A., & Cassisi, S. 2011, *A&A*, 534, A9
- Siegel, M. H., Majewski, S. R., Law, D. R., et al. 2011, *ApJ*, 743, 20
- Simioni, M., Milone, A. P., Bedin, L. R., et al. 2016, *MNRAS*, 461, 3668
- Sollima, A., & Baumgardt, H. 2017, *MNRAS*, 471, 3668
- Vesperini, E., & Heggie, D. C. 1997, *MNRAS*, 289, 898
- Vesperini, E., McMillan, S. L. W., D’Antona, F., & D’Ercole, A. 2013, *MNRAS*, 429, 1913
- Yong, D., & Grundahl, F. 2008, *ApJ*, 672, L29

APPENDIX A: EXTRA MATERIAL

In this section we complement Figures 1 and 5 with those referred to the rest of the sample. In particular, Figures A1, A2, A3, A4, A5, A6, A7 and A8 complement the sample of finding charts presented in Figure 1. Figures A9, A10, A11, A12, A13, A14, A15 and A16 are analogs to the lower-right panel of Figure 5.

This paper has been typeset from a $\text{\TeX}/\text{\LaTeX}$ file prepared by the author.

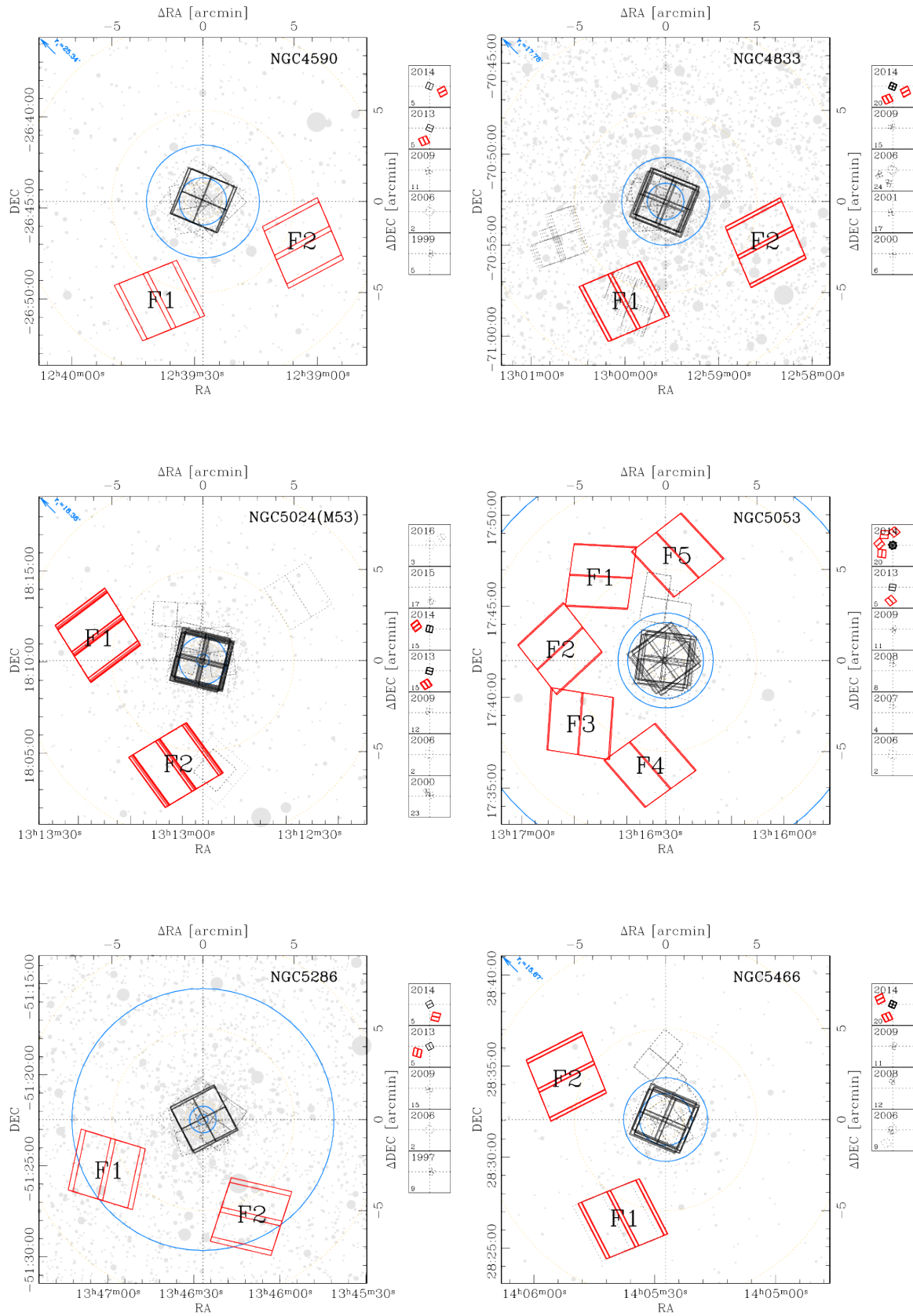


Figure A1. As in Figure 1 but for NGC 4590, NGC 4833, NGC 5024, NGC 5053, NGC 5286 and NGC 5466

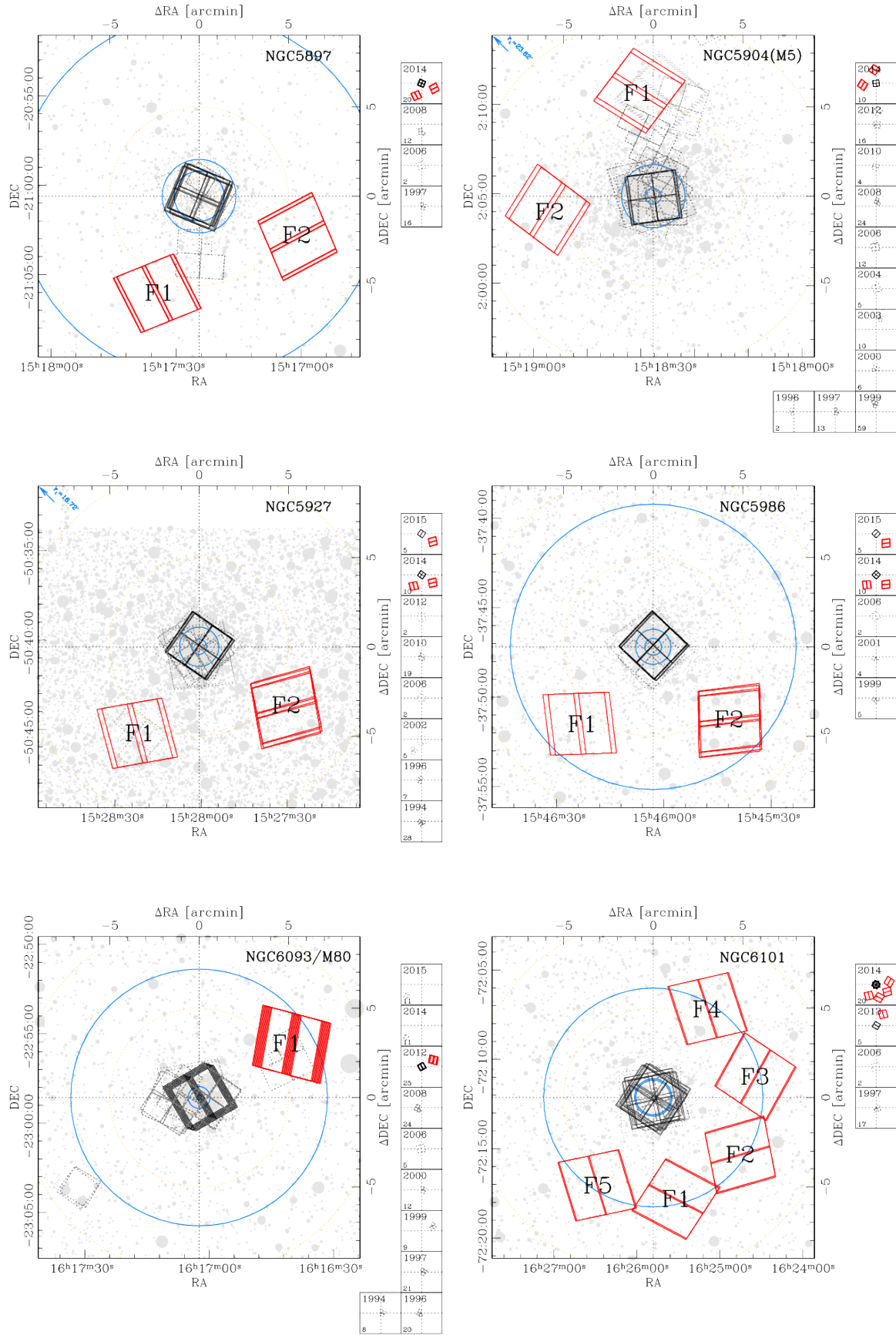


Figure A2. As in Figure 1 but for NGC 5897, NGC 5904, NGC 5927, NGC 5986, NGC 6093 and NGC 6101

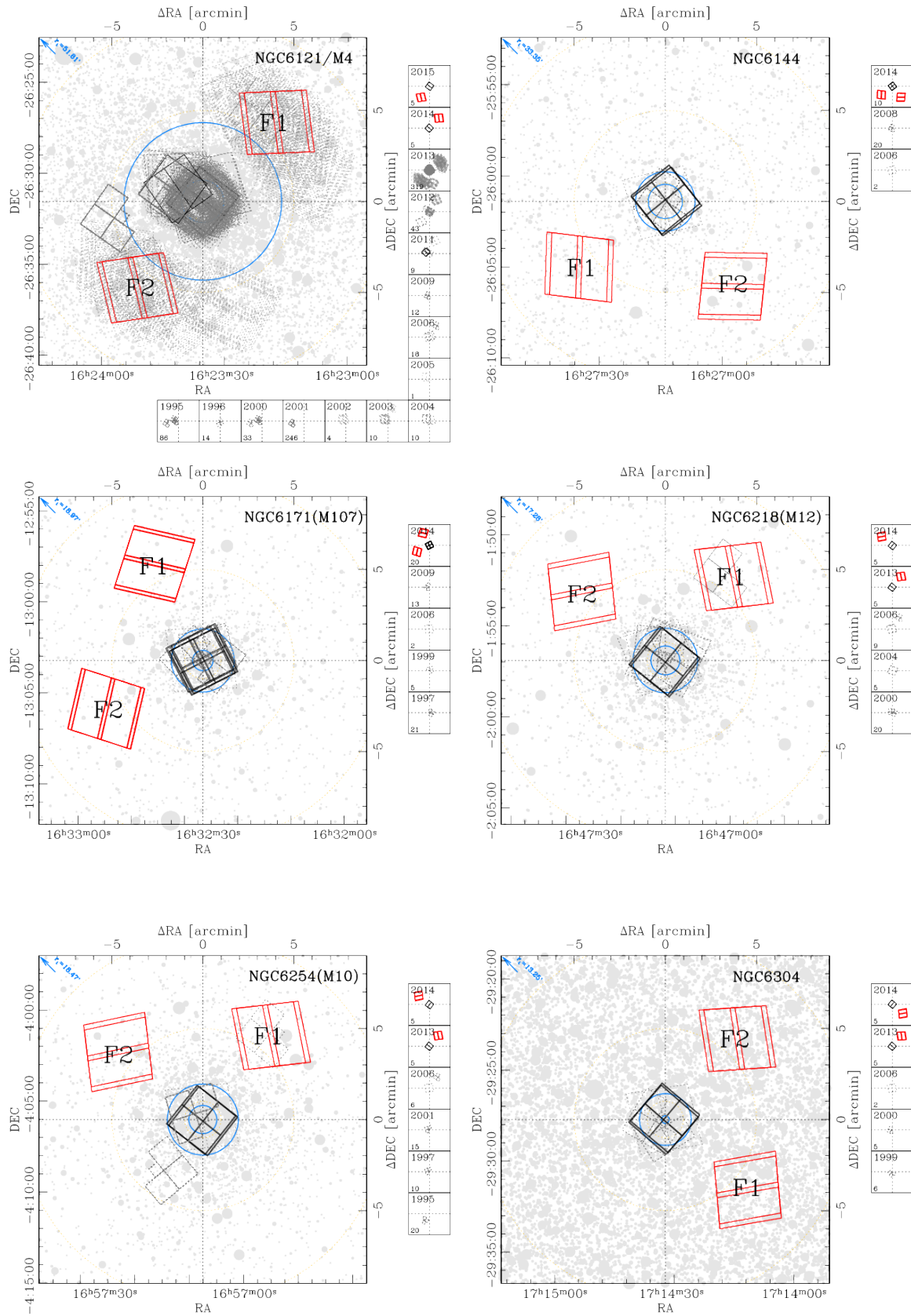


Figure A3. As in Figure 1 but for NGC 6121, NGC 6144, NGC 6171, NGC 6218, NGC 6254 and NGC 6304

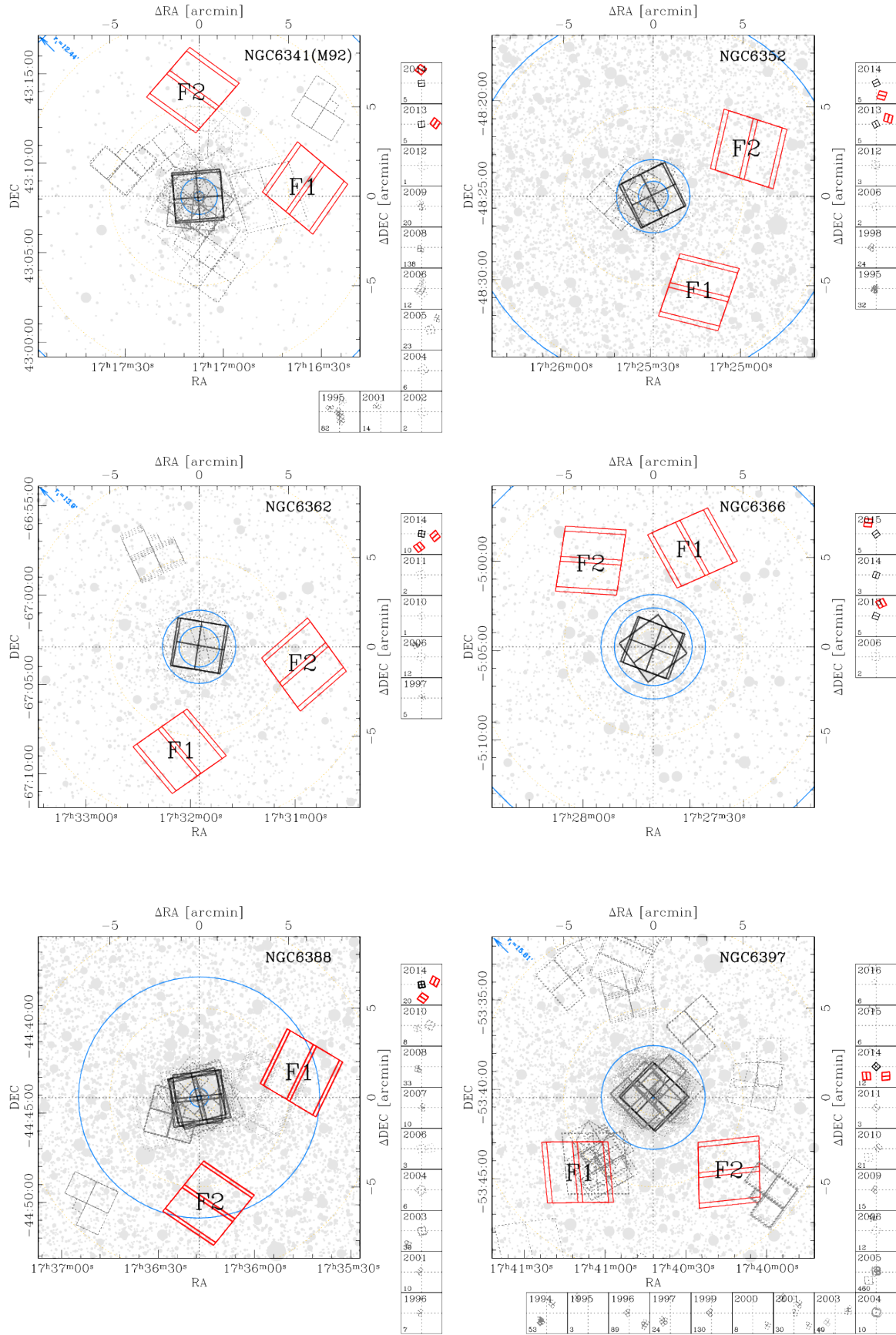


Figure A4. As in Figure 1 but for NGC 6341, NGC 6352, NGC 6362, NGC 6366, NGC 6388 and NGC 6397

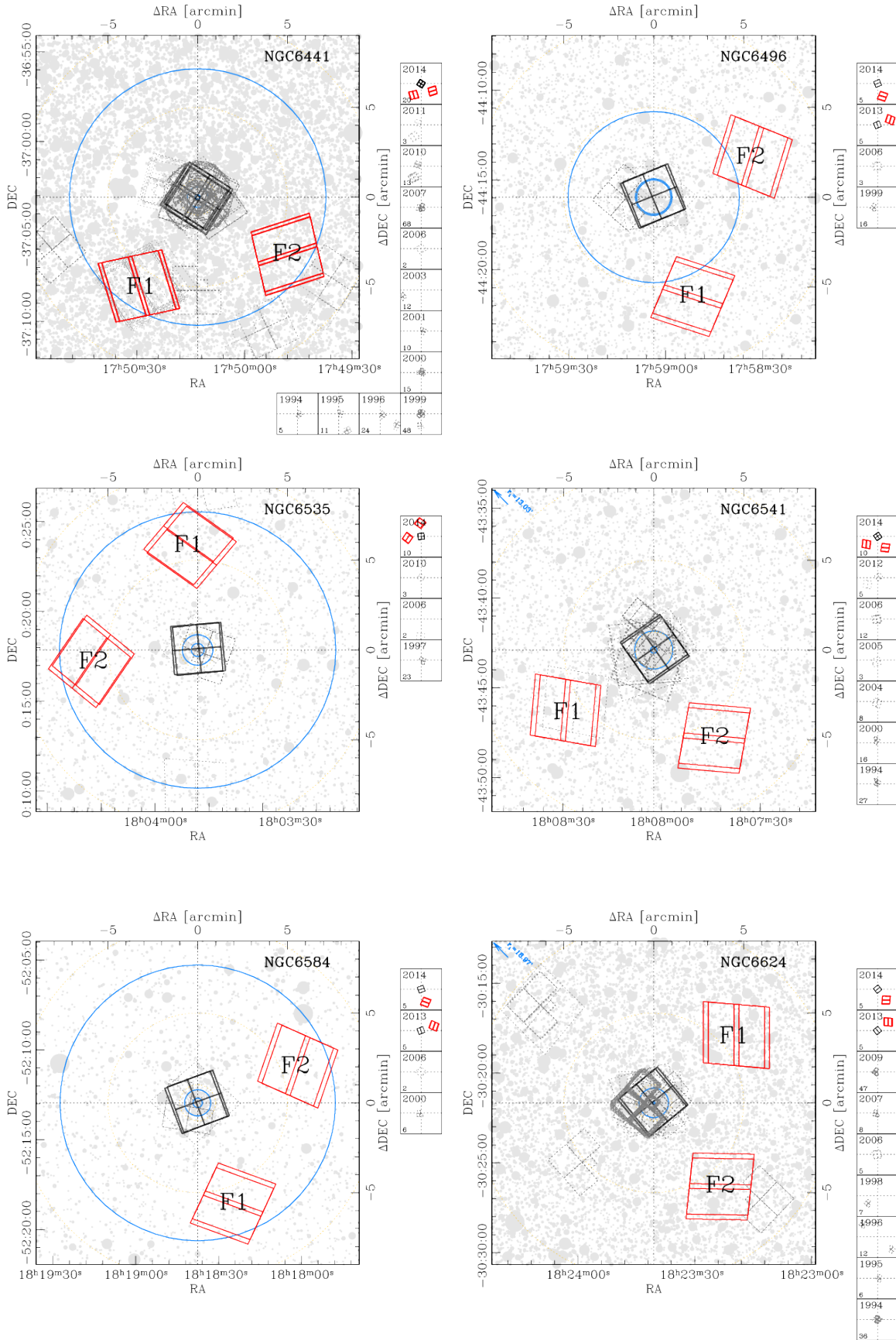


Figure A5. As in Figure 1 but for NGC 6441, NGC 6496, NGC 6535, NGC 6541, NGC 6584 and NGC 6624

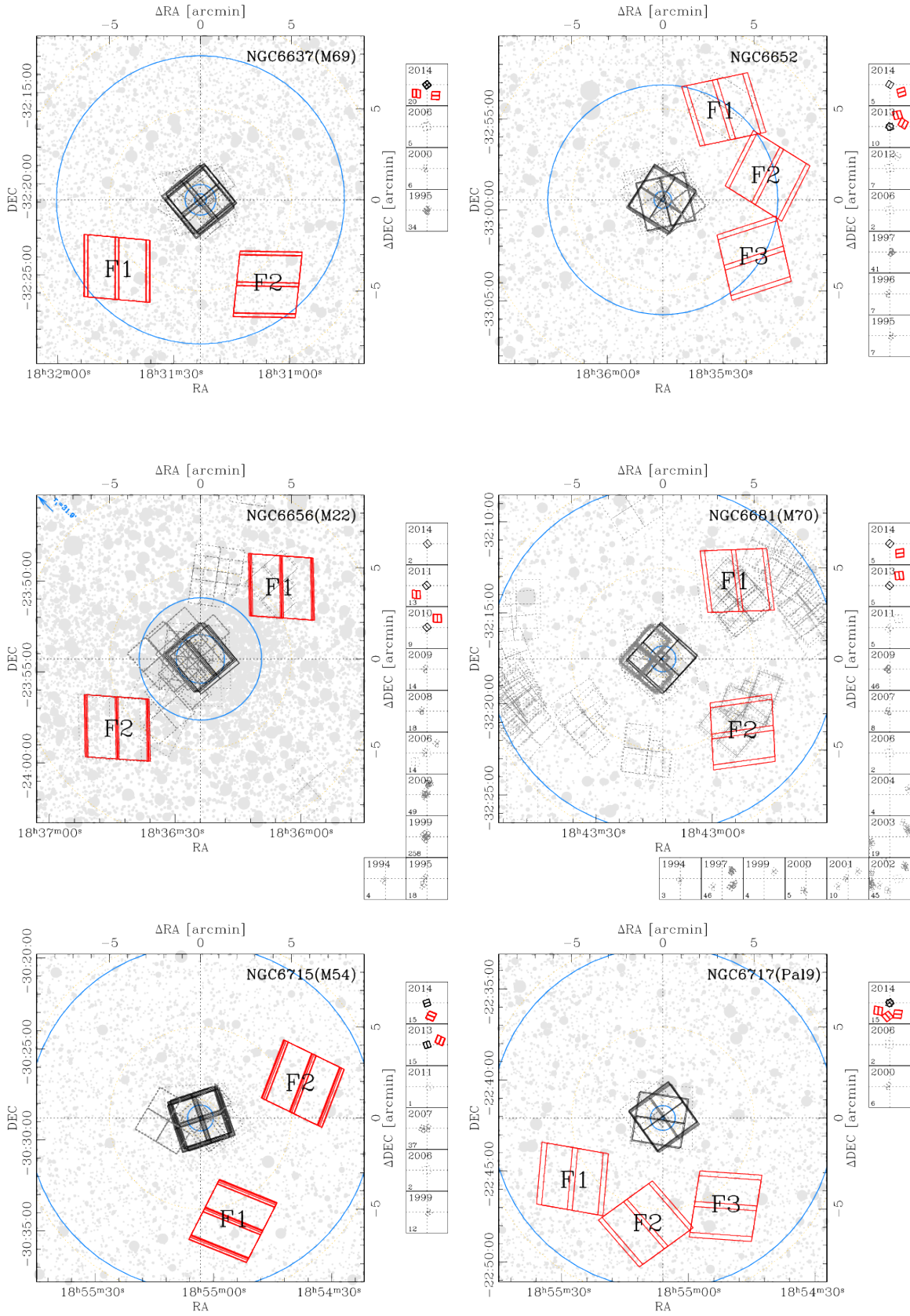


Figure A6. As in Figure 1 but for NGC 6637, NGC 6652, NGC 6656, NGC 6681, NGC 6715 and NGC 6717

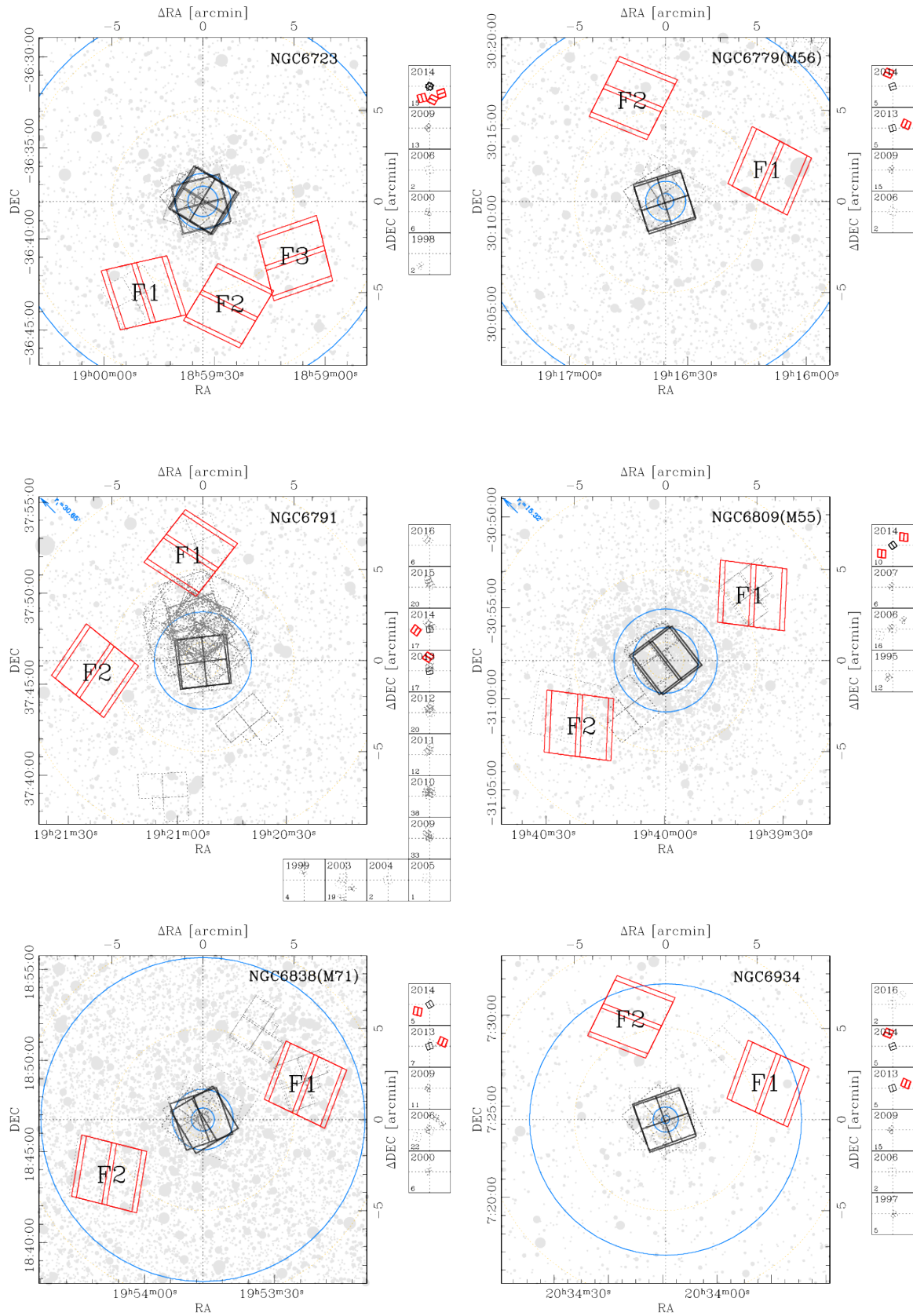


Figure A7. As in Figure 1 but for NGC 6723, NGC 6779, NGC 6791, NGC 6809, NGC 6838 and NGC 6934

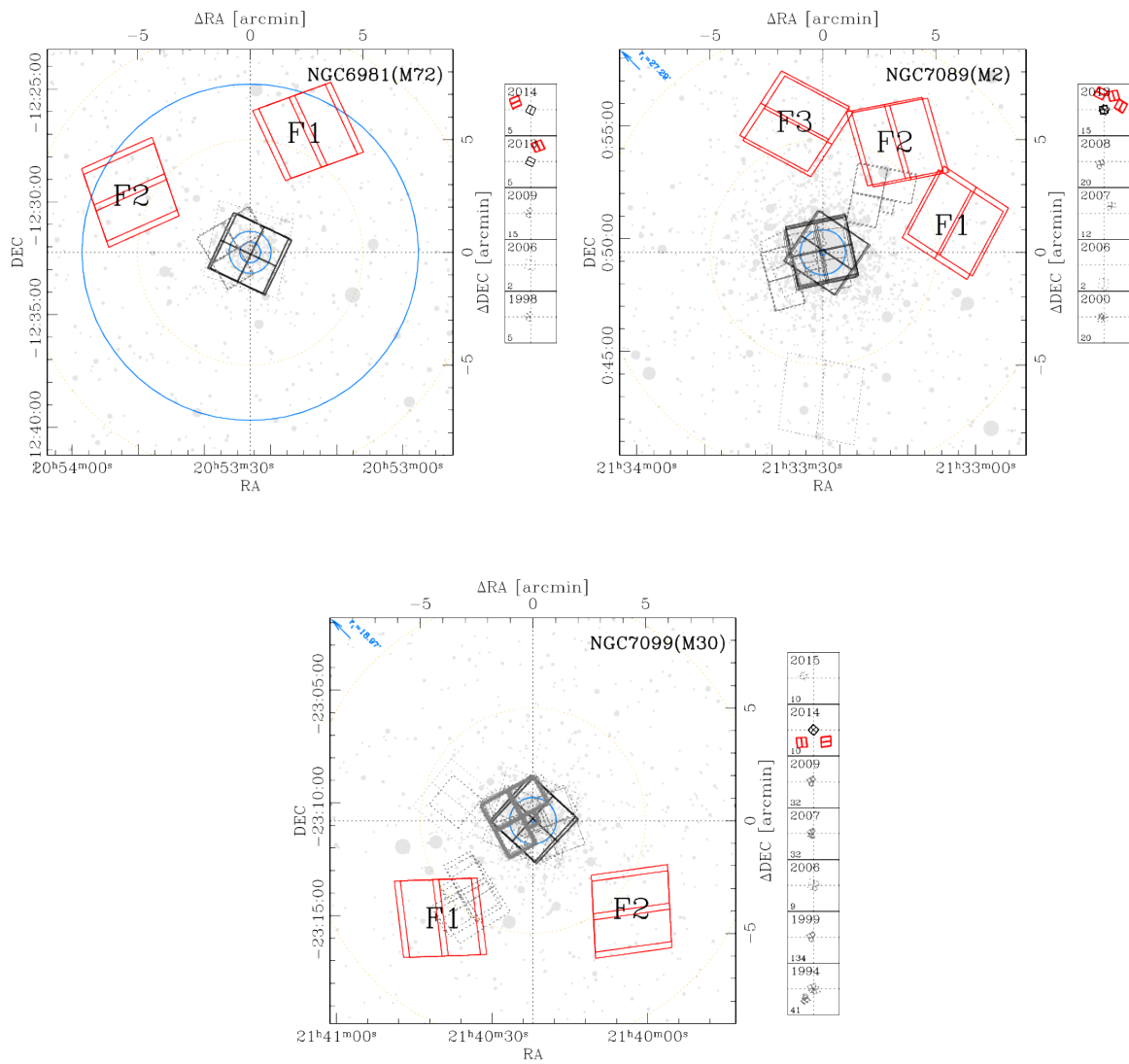


Figure A8. As in Figure 1 but for NGC 6981, NGC 7089 and NGC 7099

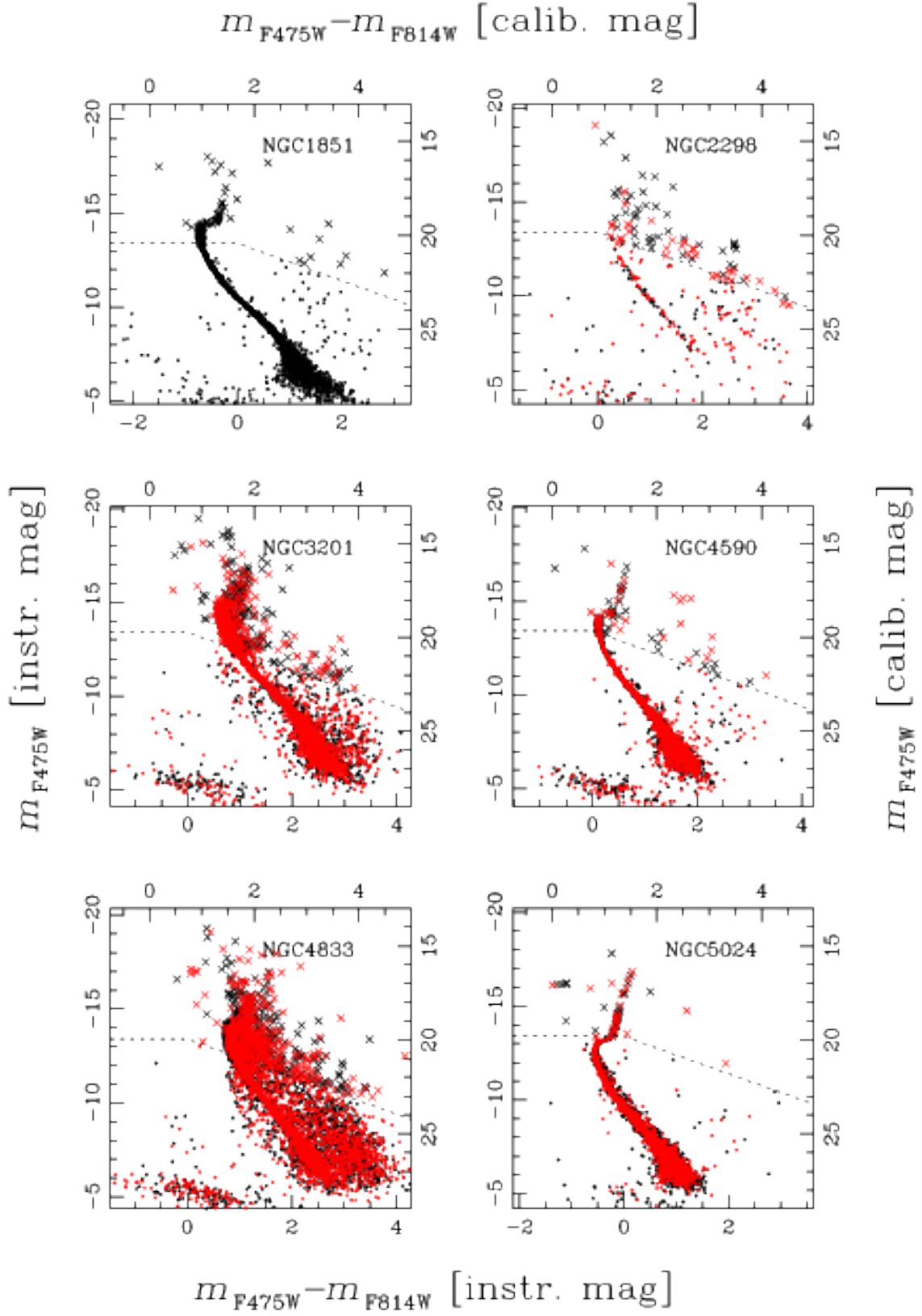


Figure A9. Obtained CMDs for NGC 1851, NGC 2298, NGC 3201, NGC 4590 and NGC 5024. For each cluster, CMDs for all fields have been merged together. The colour-code is such that black dots represent stars measured in F1; red dots, stars of F2; green dots stars of F3; blue dots stars of F4 and orange dots represent stars measured in F5. Dashed lines represent the saturation level for all F1, saturated stars are represented by crosses.

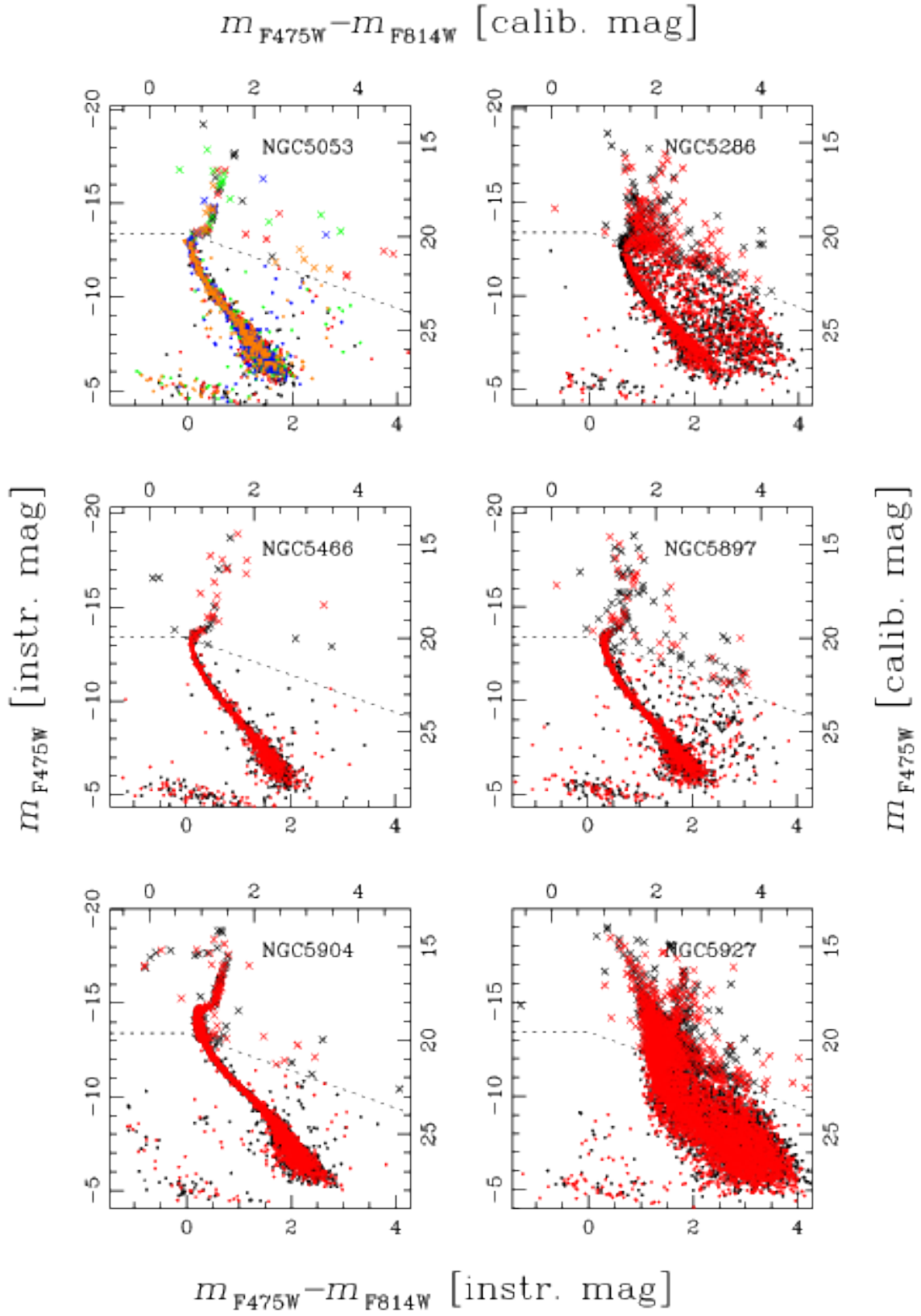


Figure A10. As in Figure A9 but for NGC 5053, NGC 5286, NGC 5466, NGC 5897, NGC 5904 and NGC 5927

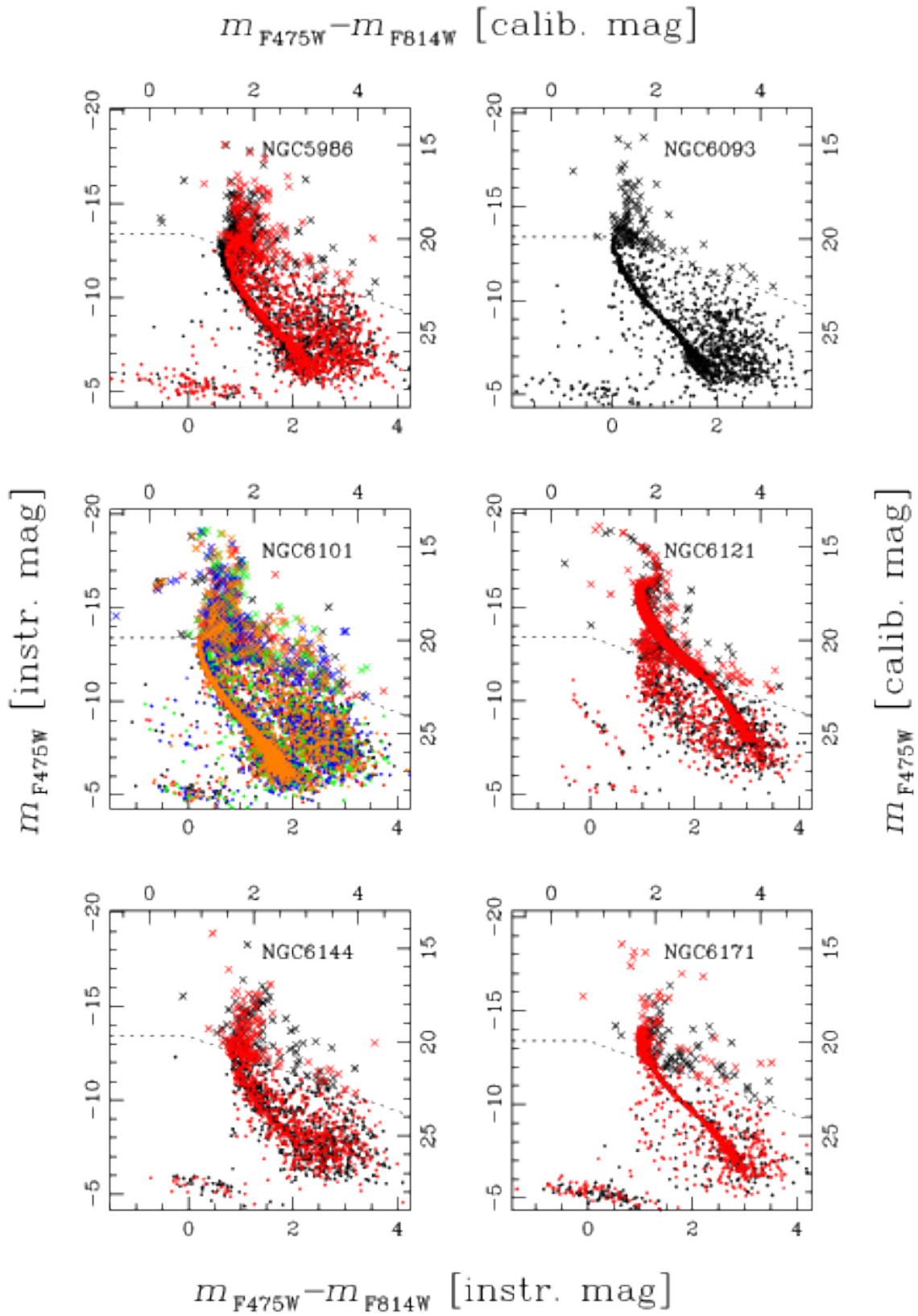


Figure A11. As in Figure A9 but for NGC 5986, NGC 6093, NGC 6101, NGC 6121, NGC 6144 and NGC 6171

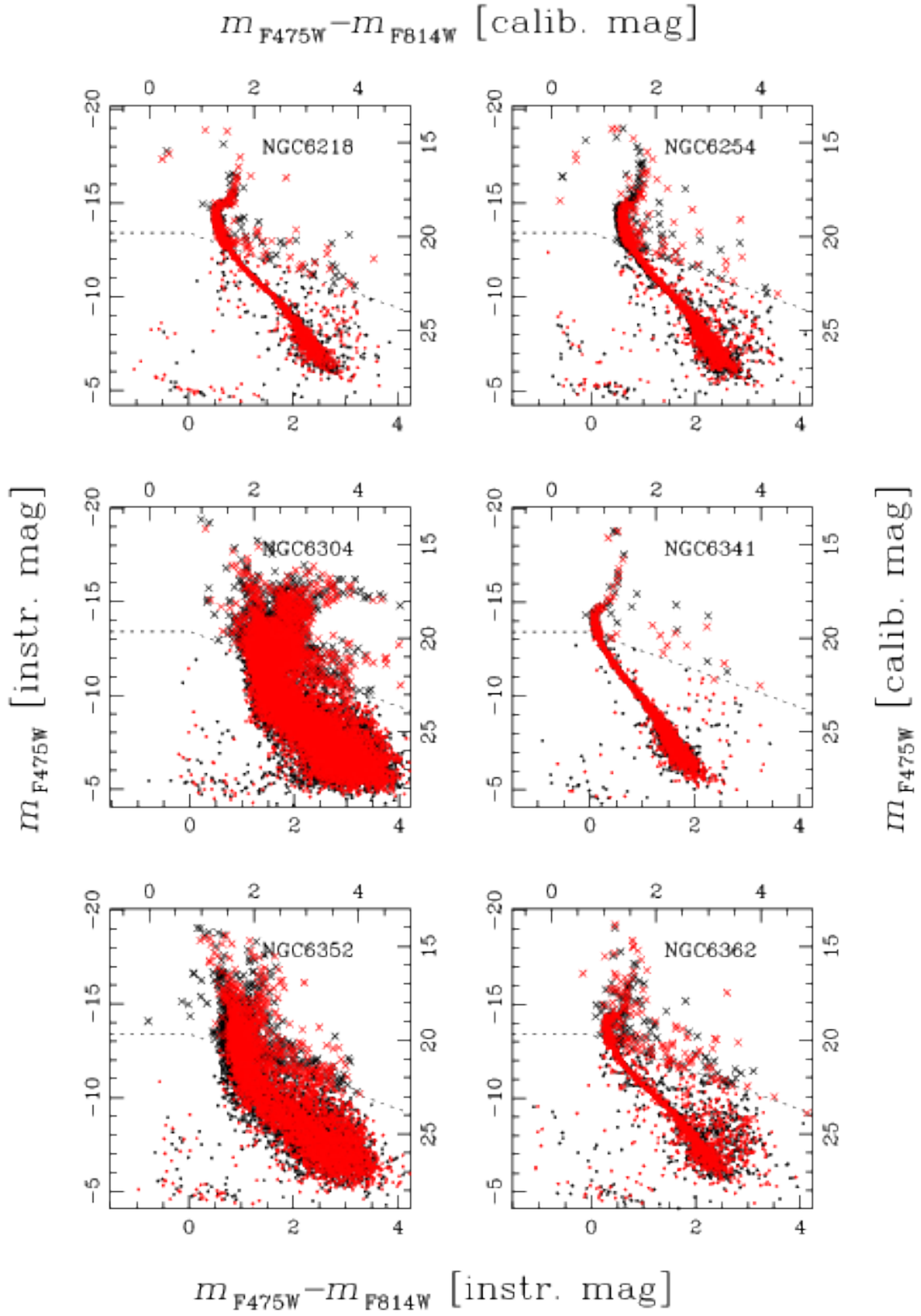


Figure A12. As in Figure A9 but for NGC 6218, NGC 6254, NGC 6304, NGC 6341, NGC 6352 and NGC 6362

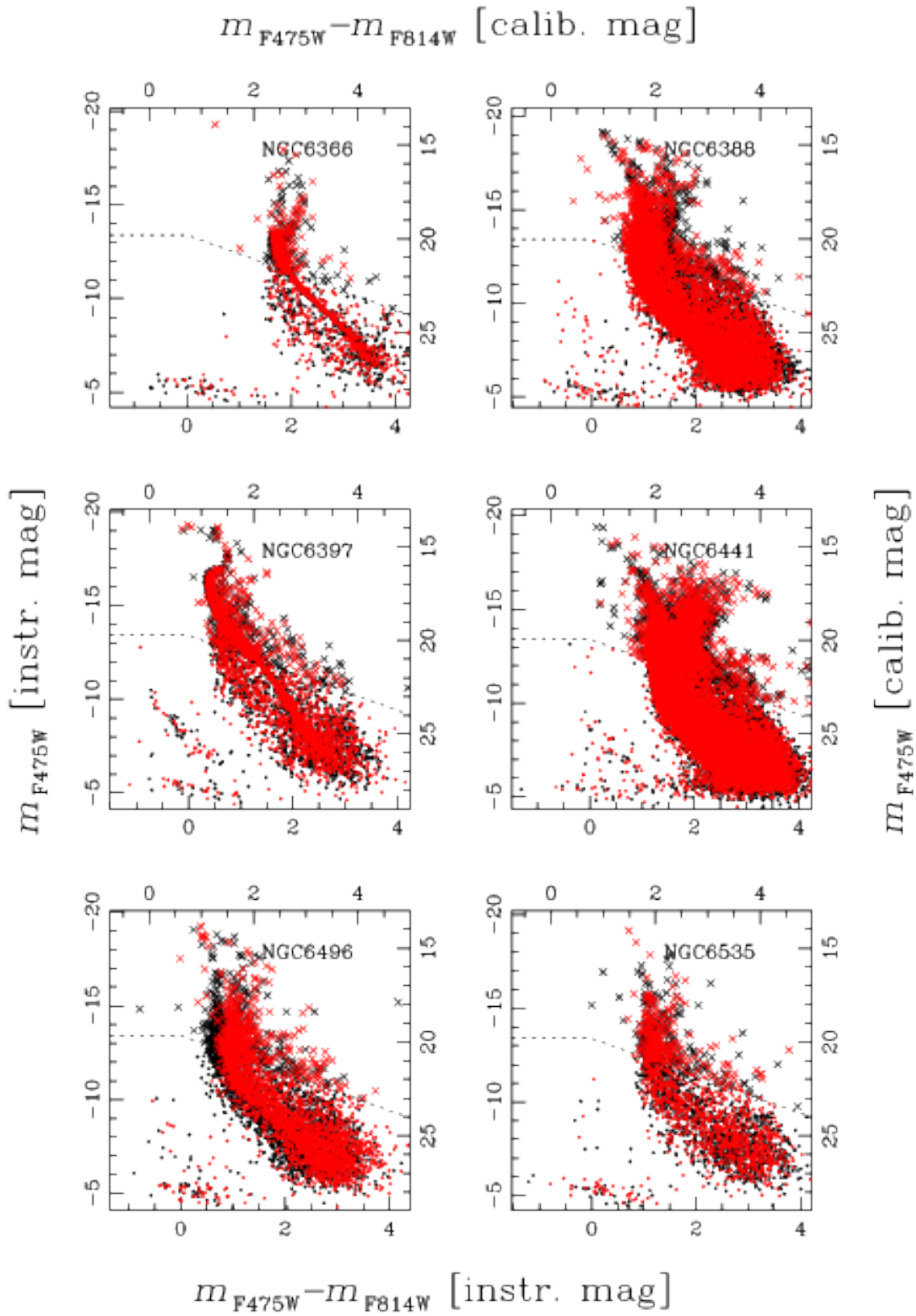


Figure A13. As in Figure A9 but for NGC 6366, NGC 6388, NGC 6397, NGC 6441, NGC 6496 and NGC 6535

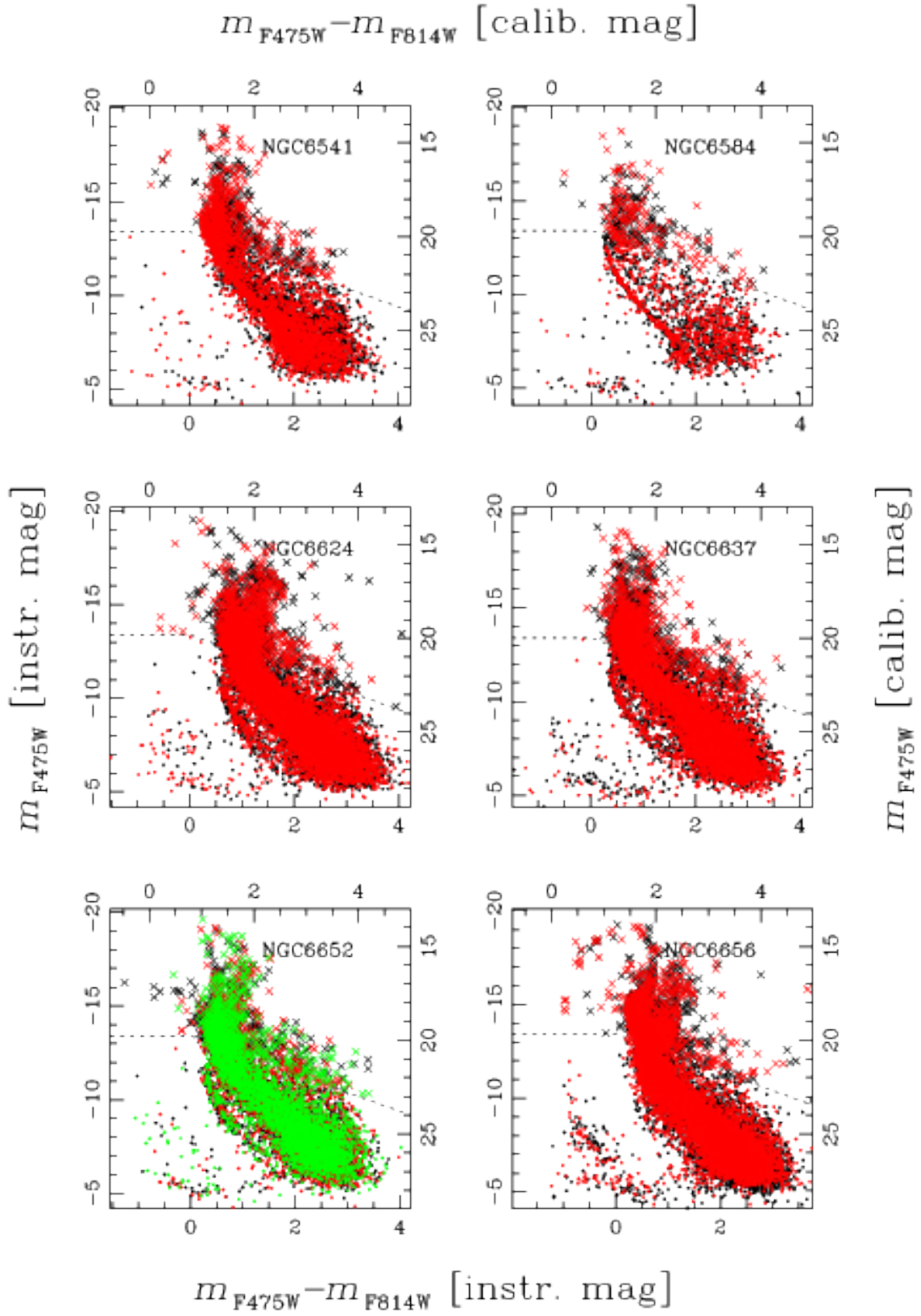


Figure A14. As in Figure A9 but for NGC 6541, NGC 6584, NGC 6624, NGC 6637, NGC 6652 and NGC 6656

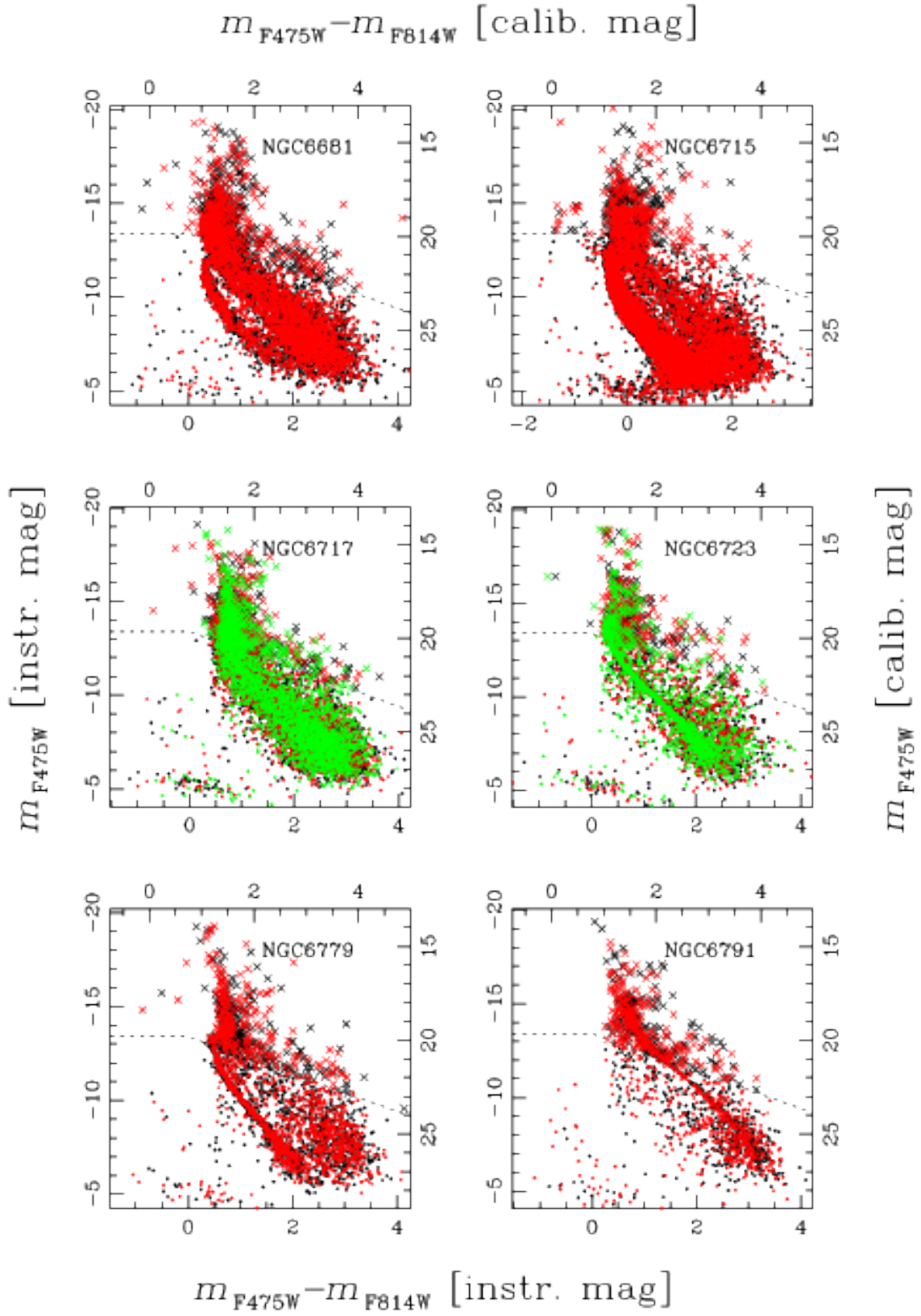


Figure A15. As in Figure A9 but for NGC 6681, NGC 6715, NGC 6717, NGC 6723, NGC 6779 and NGC 6791

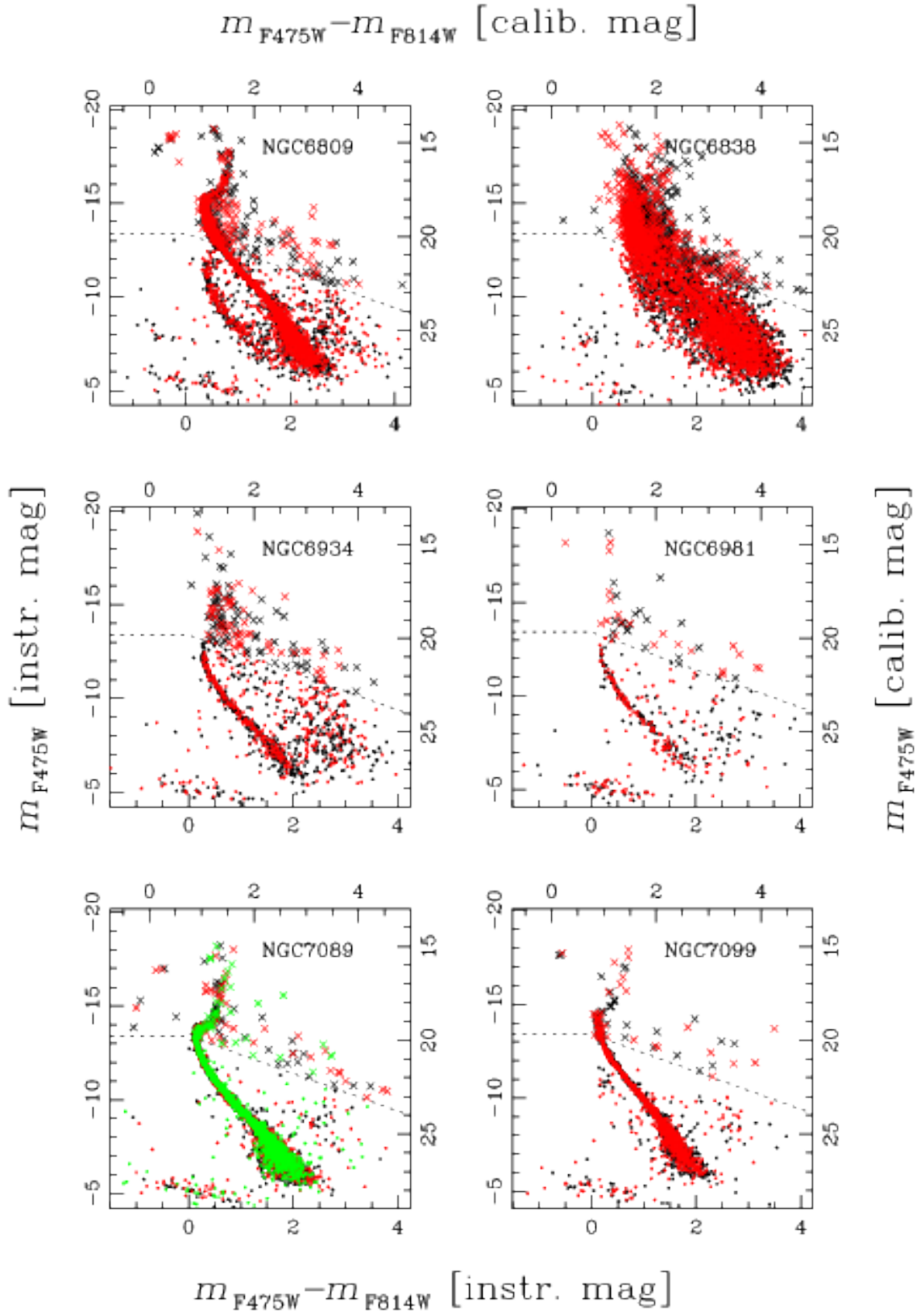


Figure A16. As in Figure A9 but for NGC 6809, NGC 6838, NGC 6934, NGC 6981, NGC 7089 and NGC 7099